Time response analysis of periodic structures via wave-based absorbing boundary conditions

D. Duhamel, J.-M. Mencik

Version of Record: https://www.sciencedirect.com/science/article/pii/S099775382100173X
Manuscript_8ef80d166466966f93442a4b6e6c561b

Time response analysis of periodic structures via wave-based absorbing boundary conditions

D. Duhamel[a,*], J.-M. Mencik[b]

[a] *Ecole des Ponts ParisTech, Laboratoire Navier, ENPC/UGE/CNRS, 6 et 8 Avenue Blaise Pascal, Cité Descartes, Champs-sur-Marne, 77455 Marne La Vallée Cedex 2, France*
[b] *INSA Centre Val de Loire, Université d'Orléans, Université de Tours, Laboratoire de Mécanique Gabriel Lamé, Rue de la Chocolaterie, 41000 Blois, France*

Abstract

A finite element procedure is proposed to compute the dynamic response of infinite periodic structures subject to localized time-dependent excitations. Straight periodic structures which are made up of cells/substructures of arbitrary shapes (e.g., 2D substructures) are analyzed. The proposed approach involves considering a periodic structure of finite length with excitation sources and absorbing boundary conditions which are expressed in the time domain. The absorbing boundary conditions are first described in the frequency domain by means of impedance matrices using a wave approach. Afterwards, they are switched to the time domain by decomposing the impedance matrices via rational functions, and expressing these rational functions in terms of polynomials of the frequency $\mathtt{i}\omega$ up to order 2. The related matrix system involves the usual vectors of displacements, velocities and accelerations, as well as vectors of supplementary variables. As such, it can be simply and quickly convert to the time domain yielding a classical second-order time differential equation which can be integrated with the Newmark algorithm. Numerical experiments are proposed which highlight the relevance of the approach.

Keywords: periodic structures, time response, absorbing boundary conditions, wave finite element method.

1. Introduction

Many engineering structures are periodic, e.g., railway tracks, pipelines, ribbed plates, metamaterials, and so on. Among these are 1D periodic structures made up of cells/substructures of arbitrary shapes (e.g., 2D substructures). Usually, these structures are analyzed in the frequency domain via different methods, e.g., the semi-analytical finite element (SAFE) method developed in [1–7] for uniform waveguides. Within this framework, the displacement solution is separated into an analytical harmonic function, along the direction of a waveguide, and a finite element (FE) field on the cross-section. Concerning the prediction of the dynamic response of truly periodic structures with non-uniform sections under harmonic loading, the wave finite element (WFE) method is a well established numerical tool. This consists in computing wave modes (propagation constants, wave shapes) of a periodic structure from the FE model of a substructure and its related mass, damping and stiffness matrices which can be obtained from any FE software or MATLAB. Afterwards, these wave modes can be used to calculate the harmonic response of periodic structures in an efficient way, i.e., by computing small matrix systems for one substructure, or a few of them. The main steps of the method can be found in [8–11].

*Corresponding author
Email addresses: denis.duhamel@enpc.fr (D. Duhamel), jean-mathieu.mencik@insa-cvl.fr (J.-M. Mencik)

Also, some of its recent extensions and applications are reported in [12–21]. So far, these studies have been conducted in the frequency domain in which the WFE method has been originally formulated.

The time response analysis of periodic structures under time-dependent excitations — e.g., fast loadings like shocks or blast — is not so well reported. For infinite structures, the main difficulty is to solve a time differential equation on a given finite domain, and therefore, be able to express appropriate (time-dependent) absorbing/infinite conditions at the boundary of this domain. Time-dependent absorbing boundary conditions (BCs) are usually formulated for homogeneous domains like acoustic or elastic media. For instance, absorbing BCs involving differential operators of different orders have been proposed in [22–25] and in [26] using sequences of local non-reflecting BCs in spherical and cylindrical coordinates. This approach has been modified to describe absorbing BCs for waves at some discrete angles from the surface normal [27, 28]. More efficient BCs can be obtained by adding supplementary variables to model an exterior surface, see [29–31]. Another possibility is the perfectly matched layer (PML) method proposed in [32–35] which consists in surrounding a computational domain with one or several layers of elements in which the wave equation is analytically continued into complex coordinates. Contrary to the previous approaches which are easy to implement but of limited accuracy, the PML method does not require analytical expressions of the absorbing BCs, but instead, one or several additional FE layers with increasing and well selected absorption properties.

Although more complex than the homogeneous case, the time domain analysis of periodic media has been carried out in various ways, mostly for electromagnetic applications. In [36, 37], PMLs have been used as absorbing BCs. In [38], it has been found, however, that the PML method can be prone to divergence issue for analyzing layered periodic electromagnetic media with evanescent waves. In [39], approximate time domain absorbing BCs have been developed for the analysis of the electromagnetic wave propagation in periodic media. Also, in [40], the time domain scattering of waves in infinite media by diffraction gratings has been conducted in a theoretical way using a Dirichlet-to-Neumann (DtN) map, without numerical results. It should be remarked that the DtN map approach involves a non-local operator which, as such, yields large sized fully-populated impedance matrices. A similar approach has been used in [41, 42]. In these works, the transient electromagnetic wave interaction with diffraction gratings has been analyzed via discontinuous Galerkin methods and exact non-local absorbing BCs for 3D periodic media. The procedure requires convolution integrals in space and time on a boundary.

Although well suited to describe absorbing BCs for homogeneous media, or simple periodic media, all of these approaches appear difficult to apply to complex systems like periodic elastic structures with arbitrary-shaped cells. Regarding the PML method, the issue mainly concerns the determination of the absorption properties of the layers to absorb waves emanating from an heterogeneous medium. Also, most of these approaches focus on the analysis of non-dispersive media having well defined wave propagation velocities. For dispersive media like beams [43], or multi-layered systems [44], absorbing BCs can be formulated in terms of boundary operators involving complicated functions of the frequency — e.g., square roots of the frequency — which, as such, cannot be converted to simple functions of time after inverse Fourier transforms. Also, these approaches appear difficult to implement given that a substantial part of the time history of the solutions must be kept, which means computing time integrals at each time step as discussed in [45]. Another strategy for describing absorbing BCs for beams involves changing the geometry at the ends by considering tapered beams [46], which, however, seems difficult to apply to more complicated structures.

Considering the potential of the WFE method for predicting the dynamic behavior of periodic structures in the frequency domain, in this work it is intended to extend this method to the time response analysis of infinite periodic structures. This, however, cannot be carried out straightforwardly. The issue is linked to the wave-based matrix equations involved in the WFE method which represent complicated functions of the frequency (i.e., $\mathtt{i}\omega$) and which do not generally possess an analytical expression. This makes any time domain transform hard to perform. The goal of the present paper is

to provide a possible answer to this question by targeting the problem of infinite 1D periodic structures subject to localized time-dependent excitations. These are structures which are frequently encountered in mechanical engineering, e.g., railway tracks or slender periodic beam-like structures. In order to stay as close as possible to a classical FE modeling, a finite FE mesh of a structure truncated at some finite extent from the excitation sources is considered (see Fig. 1). This allows analyzing the evanescent near-field effect in the vicinity of the excitations, but also, analyzing structures which are not necessarily strictly periodic in that region and which are modeled by finite elements. In this case, the coupling effect with the rest of the infinite structure — i.e., two semi-infinite periodic structures that would expand to the left and right directions at the left and right boundaries of the truncated structure — are taken into account via absorbing BCs. Although easy established in the frequency domain via the WFE method — i.e., by retaining only the waves which propagate outwards from the structure to the left or right semi-infinite structure — these absorbing BCs cannot be easily converted to the time domain for the reasons mentioned earlier.

In this paper, an original approach well suited for modeling periodic structures with absorbing BCs in the time domain is proposed. Within the FE framework, the periodic structures are usually modeled by means of vectors of displacements, velocities and accelerations. The key idea of the present work is to consider vectors of supplementary variables for modeling absorbing BCs by means of classical second-order time differential equations. In this sense, a global second-order time differential equation can be proposed for modeling a periodic structure with absorbing BCs, which can be easily integrated via the Newmark algorithm. The advantages of the proposed approach compared to the aforementioned ones are: (i) it is well adapted to the analysis of periodic structures like those made up of arbitrary-shaped substructures (e.g., 2D substructures); (ii) it can be easily implemented in an FE model and yields second-order time differential equations which are standard and easy to solve. The key steps of the proposed approach are summarized as follows. First, the absorbing BCs are expressed in the frequency domain via impedance matrices and the WFE method. Then, the impedance matrices are decomposed via rational approximations using rational functions with computed poles and matrices of residues. These rational functions can be reformulated in terms of mass, damping and stiffness matrices by using vectors of supplementary variables at the left and right boundaries of the structure in a similar way to the works in [29–31]. Finally, by assembling these new matrices together with the FE mass, damping and stiffness of the structure, this yields a classical dynamic matrix system in the time domain which can be solved by the Newmark algorithm.

The rest of the paper is organized as follows. In Sec. 2, the main steps of the WFE method are recalled. The FE modeling of a periodic structure of finite length — i.e., with a finite number of substructures — subject to time-dependent excitations and absorbing BCs at its left and right ends is presented. The related impedance matrices, in the frequency domain, are formulated. Also, the strategy to express the absorbing BCs in the time domain is proposed. The Newmark integration scheme used to solve the equation of motion of the structure is finally detailed. In Sec. 3, the proposed approach is numerically validated to predict the time response of an infinite Euler-Bernoulli beam lying on an elastic foundation and subject to a point harmonic force, where analytical solutions exist. In Sec. 4, the proposed approach is used to describe the time response of two periodic structures involving 2D substructures. Point forces of harmonic type or Ricker wavelet type (shock) are analyzed. Numerical comparisons with an equivalent infinite full FE model are brought. Concluding remarks are finally brought in Sec. 5

2. Theory

2.1. General problem

The present paper investigates the dynamic response of infinite 1D periodic structures subject to time-dependent loadings (e.g., shocks), and the modeling of such infinite structures by means of

structures of finite length and appropriate absorbing BCs for the waves escaping from excitations. For instance, a schematic of a periodic structure made up of $N = 10$ identical substructures subject to time-dependent forces and absorbing BCs is shown in Fig. 1. The substructures under concern can be of arbitrary shape — e.g., 2D substructures as shown in Fig. 2 — and are supposed to be linear, elastic, isotropic and damped (viscous damping). Also, the excitations are supposed to be confined to a part of the structure encompassing those substructures and bounded by two left and right boundaries $S_{\mathtt{L}}$ and $S_{\mathtt{R}}$, as shown in Fig. 1, where absorbing BCs are considered. From a physical point of view, these absorbing BCs mean that the energy is escaping towards infinity and that no wave comes from infinity. The purpose of the present paper is to propose a FE model which is well suited for time response analysis of such truncated periodic structures via appropriate "time-based" absorbing conditions on $S_{\mathtt{L}}$ and $S_{\mathtt{R}}$ to describe semi-infinite structures at both sides.

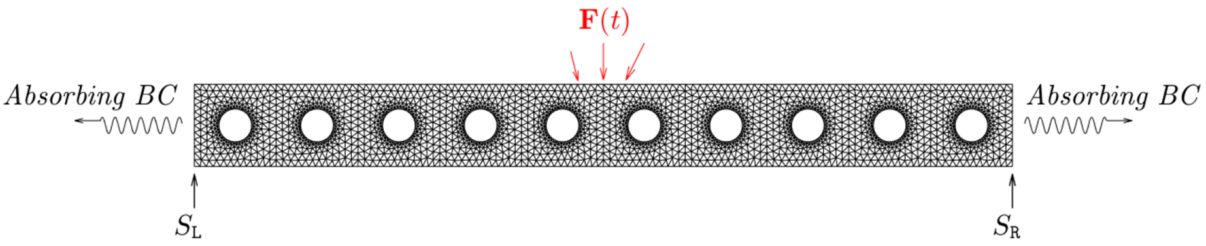

Figure 1: Schematic of a periodic structure with $N = 10$ substructures subject to time-dependent excitations and semi-infinite BCs.

2.2. WFE method

The wave propagation analysis in 1D periodic structures can be conducted with the WFE method [9, 11, 47]. The basics of the method are recalled hereafter. Let us consider infinite structures under harmonic disturbance $e^{\mathtt{i}\omega t}$ which are built from identical substructures as shown in Fig. 2. Those substructures are supposed to share the same FE mesh, and are modeled by means of identical mass, damping and stiffness matrices $\mathbf{M}^s$, $\mathbf{C}^s$ and $\mathbf{K}^s$. The related dynamic equilibrium equation is given by:

$$\mathbf{D}^s\mathbf{q}^s = \mathbf{F}^s, \tag{1}$$

where $\mathbf{q}^s$ and $\mathbf{F}^s$ refer to the displacement vector and the force vector (respectively), and where $\mathbf{D}^s$ is the dynamic stiffness matrix of the substructures (similar for all the substructures) expressed by $\mathbf{D}^s = -\omega^2\mathbf{M}^s + \mathtt{i}\omega\mathbf{C}^s + \mathbf{K}^s$.

The FE mesh of a substructure is shown in Fig. 2, and involves left ($\mathtt{L}$) and right ($\mathtt{R}$) boundaries which are described with the same number n of degrees of freedom (DOFs). Rearranging Eq. (1) yields the following transfer matrix relation between the right and left boundaries of the substructure:

$$\mathbf{u}^s_{\mathtt{R}} = \mathbf{S}^s\mathbf{u}^s_{\mathtt{L}}, \tag{2}$$

where $\mathbf{u}^s_{\mathtt{R}}$ and $\mathbf{u}^s_{\mathtt{L}}$ are $2n \times 1$ state vectors expressed by:

$$\mathbf{u}^s_{\mathtt{R}} = \begin{bmatrix} \mathbf{q}^s_{\mathtt{R}} \\ \mathbf{F}^s_{\mathtt{R}} \end{bmatrix} \quad , \quad \mathbf{u}^s_{\mathtt{L}} = \begin{bmatrix} \mathbf{q}^s_{\mathtt{L}} \\ -\mathbf{F}^s_{\mathtt{L}} \end{bmatrix}. \tag{3}$$

Also, $\mathbf{S}^s$ is a symplectic $2n \times 2n$ matrix (also called transfer matrix) expressed by:

$$\mathbf{S}^s = \left[\begin{array}{c|c} -(\mathbf{D}^{s*}_{\mathtt{LR}})^{-1}\mathbf{D}^{s*}_{\mathtt{LL}} & -(\mathbf{D}^{s*}_{\mathtt{LR}})^{-1} \\ \hline \mathbf{D}^{s*}_{\mathtt{RL}} - \mathbf{D}^{s*}_{\mathtt{RR}}(\mathbf{D}^{s*}_{\mathtt{LR}})^{-1}\mathbf{D}^{s*}_{\mathtt{LL}} & -\mathbf{D}^{s*}_{\mathtt{RR}}(\mathbf{D}^{s*}_{\mathtt{LR}})^{-1} \end{array}\right], \tag{4}$$

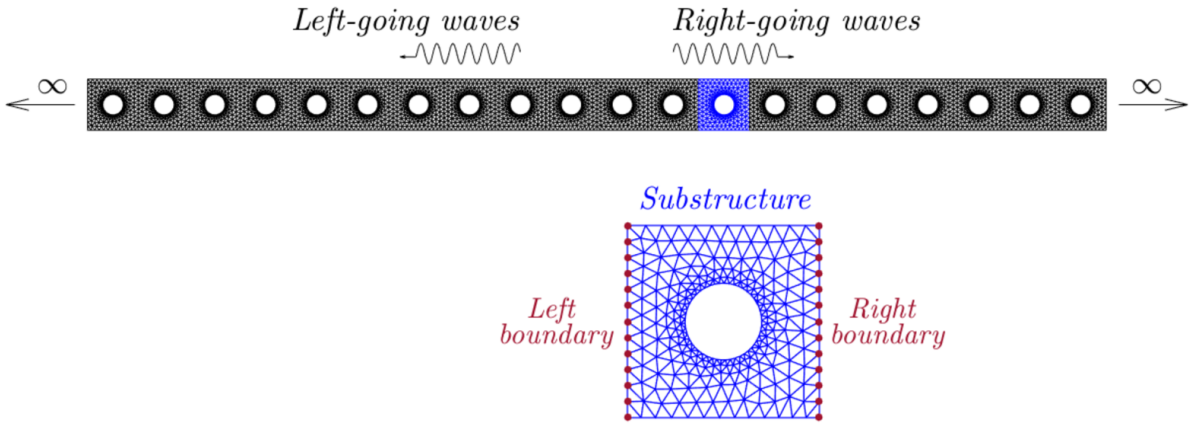

Figure 2: Periodic structure of infinite length, and FE mesh of a substructure.

where $\mathbf{D}^{s*}$ refers to the dynamic stiffness matrix of the substructure condensed on the left and right boundaries [13].

The eigenvalues and eigenvectors of the transfer matrix $\mathbf{S}^s$ occur in pairs as $(\mu_j, \boldsymbol{\phi}_j)$ and $(\mu_j^\star = 1/\mu_j, \boldsymbol{\phi}_j^\star)$ with $|\mu_j| < 1$ (see [10] for further details about the computation of the eigensolutions of $\mathbf{S}^s$). Let us denote by d the substructure length, i.e., along the main direction of the periodic structure. According to the Bloch's theorem [48], the eigenvalues of $\mathbf{S}^s$ have the meaning of wave parameters which are given by $\mu_j = e^{-\mathtt{i}k_j d}$ and $\mu_j^\star = e^{\mathtt{i}k_j d}$ (k_j being the wavenumbers); also, the eigenvectors $\boldsymbol{\phi}_j$ (resp. $\boldsymbol{\phi}_j^\star$) have the meaning of wave shapes, for the waves traveling to the right and left directions (respectively) of the periodic structure. Those vectors of wave shapes are of size $2n \times 1$ and are usually partitioned as follows:

$$\boldsymbol{\phi}_j = \begin{bmatrix} \boldsymbol{\phi}_{\mathtt{q}j} \\ \boldsymbol{\phi}_{\mathtt{F}j} \end{bmatrix} \quad , \quad \boldsymbol{\phi}_j^\star = \begin{bmatrix} \boldsymbol{\phi}_{\mathtt{q}j}^\star \\ \boldsymbol{\phi}_{\mathtt{F}j}^\star \end{bmatrix}, \tag{5}$$

where $\boldsymbol{\phi}_{\mathtt{q}j}$ and $\boldsymbol{\phi}_{\mathtt{q}j}^\star$ (resp. $\boldsymbol{\phi}_{\mathtt{F}j}$ and $\boldsymbol{\phi}_{\mathtt{F}j}^\star$) are $n \times 1$ vectors involving displacement (resp. force) components. The related $n \times n$ matrices of wave shapes — namely, $\boldsymbol{\Phi}_{\mathtt{q}}$, $\boldsymbol{\Phi}_{\mathtt{q}}^\star$, $\boldsymbol{\Phi}_{\mathtt{F}}$ and $\boldsymbol{\Phi}_{\mathtt{F}}^\star$ — are given by:

$$\boldsymbol{\Phi}_{\mathtt{q}} = [\boldsymbol{\phi}_{\mathtt{q}1} \cdots \boldsymbol{\phi}_{\mathtt{q}n}] \quad , \quad \boldsymbol{\Phi}_{\mathtt{q}}^\star = [\boldsymbol{\phi}_{\mathtt{q}1}^\star \cdots \boldsymbol{\phi}_{\mathtt{q}n}^\star] \quad , \quad \boldsymbol{\Phi}_{\mathtt{F}} = [\boldsymbol{\phi}_{\mathtt{F}1} \cdots \boldsymbol{\phi}_{\mathtt{F}n}] \quad , \quad \boldsymbol{\Phi}_{\mathtt{F}}^\star = [\boldsymbol{\phi}_{\mathtt{F}1}^\star \cdots \boldsymbol{\phi}_{\mathtt{F}n}^\star]. \tag{6}$$

2.3. Absorbing boundary conditions in the frequency domain

Consider a periodic structure involving a finite number N of substructures which is enclosed between two left and right boundaries $S_{\mathtt{L}}$ and $S_{\mathtt{R}}$ where absorbing BCs are considered (see Fig. 1). Such BCs are used to describe the coupling effect between the periodic structure and two semi-infinite periodic structures, not shown here, that would expand to the left and right directions. The related impedance matrices for the left and right boundaries $S_{\mathtt{L}}$ and $S_{\mathtt{R}}$ — namely, $\mathbf{Z}_{\mathtt{L}}$ and $\mathbf{Z}_{\mathtt{R}}$ — can be defined, in the frequency domain, as follows:

$$\mathbf{F}_{\mathtt{L}} = \mathbf{Z}_{\mathtt{L}} \mathbf{q}_{\mathtt{L}} \quad , \quad \mathbf{F}_{\mathtt{R}} = \mathbf{Z}_{\mathtt{R}} \mathbf{q}_{\mathtt{R}}, \tag{7}$$

where $\mathbf{q}_{\mathtt{L}}$ and $\mathbf{q}_{\mathtt{R}}$ (resp. $\mathbf{F}_{\mathtt{L}}$ and $\mathbf{F}_{\mathtt{R}}$) are the displacement (resp. force) vectors (size $n \times 1$) for the periodic structure on $S_{\mathtt{L}}$ and $S_{\mathtt{R}}$. Following the WFE procedure and expanding those vectors on the

basis of wave shapes, this yields [13]:

$$\mathbf{q}_{\mathtt{L}} = \mathbf{\Phi}_{\mathtt{q}}^{\star}\mathbf{Q}_{\mathtt{L}}^{\star} \quad , \quad \mathbf{q}_{\mathtt{R}} = \mathbf{\Phi}_{\mathtt{q}}\mathbf{Q}_{\mathtt{R}}, \tag{8}$$

and

$$\mathbf{F}_{\mathtt{L}} = -\mathbf{\Phi}_{\mathtt{F}}^{\star}\mathbf{Q}_{\mathtt{L}}^{\star} \quad , \quad \mathbf{F}_{\mathtt{R}} = \mathbf{\Phi}_{\mathtt{F}}\mathbf{Q}_{\mathtt{R}}, \tag{9}$$

where $\mathbf{Q}_{\mathtt{L}}^{\star}$ (resp. $\mathbf{Q}_{\mathtt{R}}$) is the vector of wave amplitudes, at position $S_{\mathtt{L}}$ (resp. $S_{\mathtt{R}}$), for the waves traveling to the left (resp. right) direction of the structure. The fact that left-going (resp. right-going) waves are only considered at $S_{\mathtt{L}}$ (resp. $S_{\mathtt{R}}$) results from the absorbing BC, i.e., the fact that no wave comes from infinity. Eq. (8) yields $\mathbf{Q}_{\mathtt{L}}^{\star} = (\mathbf{\Phi}_{\mathtt{q}}^{\star})^{-1}\mathbf{q}_{\mathtt{L}}$ and $\mathbf{Q}_{\mathtt{R}} = (\mathbf{\Phi}_{\mathtt{q}})^{-1}\mathbf{q}_{\mathtt{R}}$ and, therefore, the following expressions for the impedance matrices:

$$\mathbf{Z}_{\mathtt{L}} = -\mathbf{\Phi}_{\mathtt{F}}^{\star}(\mathbf{\Phi}_{\mathtt{q}}^{\star})^{-1} \quad , \quad \mathbf{Z}_{\mathtt{R}} = \mathbf{\Phi}_{\mathtt{F}}(\mathbf{\Phi}_{\mathtt{q}})^{-1}. \tag{10}$$

Note that, withing the WFE framework, $\mathbf{\Phi}_{\mathtt{q}}$, $\mathbf{\Phi}_{\mathtt{q}}^{\star}$, $\mathbf{\Phi}_{\mathtt{F}}$ and $\mathbf{\Phi}_{\mathtt{F}}^{\star}$, and therefore $\mathbf{Z}_{\mathtt{L}}$ and $\mathbf{Z}_{\mathtt{R}}$, are matrix-valued functions of the frequency/pulsation ω (or $\mathtt{i}\omega$). The thing is, the dependency of these matrices on $\mathtt{i}\omega$ is not straightforward, i.e., complicated functions which do not generally possess an analytical expression. The issue is linked to the numerical steps involved in the WFE method (derivation of a transfer matrix, resolution of an eigenproblem, among others) which makes these matrix-valued functions hard to figure out. To solve this problem, it is proposed to recast Eq. (7) as two alternative matrix equations involving new impedance matrices which are simply described in terms of second-order polynomials of $\mathtt{i}\omega$. This provides a simple way to express absorbing BCs, for the periodic structure, in the time domain. The strategy is explained as follows.

Let us decompose the impedance matrices $\mathbf{Z}_{\mathtt{L}}$ and $\mathbf{Z}_{\mathtt{R}}$ via rational approximations (following similar ideas as in [49–51] for approximating transfer functions):

$$\mathbf{Z}_{\mathtt{L}} = \sum_{k=1}^{P} \frac{\mathbf{R}_{\mathtt{L}k}}{\mathtt{i}\omega - p_{\mathtt{L}k}} + \mathbf{K}_{\mathtt{L}} \quad , \quad \mathbf{Z}_{\mathtt{R}} = \sum_{k=1}^{P} \frac{\mathbf{R}_{\mathtt{R}k}}{\mathtt{i}\omega - p_{\mathtt{R}k}} + \mathbf{K}_{\mathtt{R}}, \tag{11}$$

where $p_{\mathtt{L}k}$ and $p_{\mathtt{R}k}$ denote poles ($k = 1, \ldots, P$), and $\mathbf{R}_{\mathtt{L}k}$ and $\mathbf{R}_{\mathtt{R}k}$ denote matrices of residues. Some of these usually appear in conjugate pairs, i.e., $(p_{\mathtt{L}k}, \overline{p_{\mathtt{L}k}})$ and $(p_{\mathtt{R}k}, \overline{p_{\mathtt{R}k}})$, and $(\mathbf{R}_{\mathtt{L}k}, \overline{\mathbf{R}_{\mathtt{L}k}})$ and $(\mathbf{R}_{\mathtt{R}k}, \overline{\mathbf{R}_{\mathtt{R}k}})$. In this case, it can be easily proven that:

$$\begin{aligned}
\frac{\mathbf{R}_{\mathtt{L}k}}{\mathtt{i}\omega - p_{\mathtt{L}k}} + \frac{\overline{\mathbf{R}_{\mathtt{L}k}}}{\mathtt{i}\omega - \overline{p_{\mathtt{L}k}}} &= 2\frac{\mathtt{i}\omega\Re\{\mathbf{R}_{\mathtt{L}k}\} - \Re\{\overline{p_{\mathtt{L}k}}\mathbf{R}_{\mathtt{L}k}\}}{-\omega^2 - 2\mathtt{i}\omega\Re\{p_{\mathtt{L}k}\} + |p_{\mathtt{L}k}|^2}, \\
\frac{\mathbf{R}_{\mathtt{R}k}}{\mathtt{i}\omega - p_{\mathtt{R}k}} + \frac{\overline{\mathbf{R}_{\mathtt{R}k}}}{\mathtt{i}\omega - \overline{p_{\mathtt{R}k}}} &= 2\frac{\mathtt{i}\omega\Re\{\mathbf{R}_{\mathtt{R}k}\} - \Re\{\overline{p_{\mathtt{R}k}}\mathbf{R}_{\mathtt{R}k}\}}{-\omega^2 - 2\mathtt{i}\omega\Re\{p_{\mathtt{R}k}\} + |p_{\mathtt{R}k}|^2}.
\end{aligned} \tag{12}$$

As a result, Eq. (11) leads to:

$$\begin{aligned}
\mathbf{Z}_{\mathtt{L}} &= \sum_{k=1}^{Q} 2\frac{\mathtt{i}\omega\Re\{\mathbf{R}_{\mathtt{L}(2k)}\} - \Re\{\overline{p_{\mathtt{L}(2k)}}\mathbf{R}_{\mathtt{L}(2k)}\}}{-\omega^2 - 2\mathtt{i}\omega\Re\{p_{\mathtt{L}(2k)}\} + |p_{\mathtt{L}(2k)}|^2} + \sum_{k=2Q+1}^{P} \frac{\mathbf{R}_{\mathtt{L}k}}{\mathtt{i}\omega - p_{\mathtt{L}k}} + \mathbf{K}_{\mathtt{L}}, \\
\mathbf{Z}_{\mathtt{R}} &= \sum_{k=1}^{Q} 2\frac{\mathtt{i}\omega\Re\{\mathbf{R}_{\mathtt{R}(2k)}\} - \Re\{\overline{p_{\mathtt{R}(2k)}}\mathbf{R}_{\mathtt{R}(2k)}\}}{-\omega^2 - 2\mathtt{i}\omega\Re\{p_{\mathtt{R}(2k)}\} + |p_{\mathtt{R}(2k)}|^2} + \sum_{k=2Q+1}^{P} \frac{\mathbf{R}_{\mathtt{R}k}}{\mathtt{i}\omega - p_{\mathtt{R}k}} + \mathbf{K}_{\mathtt{R}},
\end{aligned} \tag{13}$$

where $2Q < P$. To remove the denominator terms in Eq. (13), let us introduce $n \times 1$ vectors of

supplementary variables $\mathbf{X}_{\mathtt{L}k}$ and $\mathbf{X}_{\mathtt{R}k}$, and let us rewrite Eq. (7) by means of Eq. (13) as follows:

$$\begin{aligned}
\mathbf{F}_{\mathtt{L}} &= \sum_{k=1}^{Q} 2\left(\mathtt{i}\omega\Re\{\mathbf{R}_{\mathtt{L}(2k)}\} - \Re\{\overline{p_{\mathtt{L}(2k)}}\mathbf{R}_{\mathtt{L}(2k)}\}\right)\mathbf{X}_{\mathtt{L}k} + \sum_{k=2Q+1}^{P} \mathbf{R}_{\mathtt{L}k}(\mathtt{i}\omega)\mathbf{X}_{\mathtt{L}(k-Q)} + \mathbf{K}_{\mathtt{L}}\mathbf{q}_{\mathtt{L}},\\
\mathbf{F}_{\mathtt{R}} &= \sum_{k=1}^{Q} 2\left(\mathtt{i}\omega\Re\{\mathbf{R}_{\mathtt{R}(2k)}\} - \Re\{\overline{p_{\mathtt{R}(2k)}}\mathbf{R}_{\mathtt{R}(2k)}\}\right)\mathbf{X}_{\mathtt{R}k} + \sum_{k=2Q+1}^{P} \mathbf{R}_{\mathtt{R}k}(\mathtt{i}\omega)\mathbf{X}_{\mathtt{R}(k-Q)} + \mathbf{K}_{\mathtt{R}}\mathbf{q}_{\mathtt{R}},
\end{aligned} \tag{14}$$

where:

$$\begin{aligned}
&\left(-\omega^2 - 2\mathtt{i}\omega\Re\{p_{\mathtt{L}(2k)}\} + |p_{\mathtt{L}(2k)}|^2\right)\mathbf{X}_{\mathtt{L}k} = \mathbf{q}_{\mathtt{L}} \qquad \text{for } k = 1,\ldots,Q,\\
&\left(-\omega^2 - 2\mathtt{i}\omega\Re\{p_{\mathtt{R}(2k)}\} + |p_{\mathtt{R}(2k)}|^2\right)\mathbf{X}_{\mathtt{R}k} = \mathbf{q}_{\mathtt{R}} \qquad \text{for } k = 1,\ldots,Q,\\
&(-\omega^2 - \mathtt{i}\omega p_{\mathtt{L}k})\mathbf{X}_{\mathtt{L}(k-Q)} = \mathbf{q}_{\mathtt{L}} \qquad \text{for } k = (2Q+1),\ldots,P,\\
&(-\omega^2 - \mathtt{i}\omega p_{\mathtt{R}k})\mathbf{X}_{\mathtt{R}(k-Q)} = \mathbf{q}_{\mathtt{R}} \qquad \text{for } k = (2Q+1),\ldots,P.
\end{aligned} \tag{15}$$

Finally, let us introduce the following $(P-Q)n \times 1$ vectors $\mathbf{X}_{\mathtt{L}}$ and $\mathbf{X}_{\mathtt{R}}$ defined by:

$$\mathbf{X}_{\mathtt{L}} = \left[\begin{array}{c} \mathbf{X}_{\mathtt{L}1} \\ \vdots \\ \mathbf{X}_{\mathtt{L}Q} \\ \hline \mathbf{X}_{\mathtt{L}(Q+1)} \\ \vdots \\ \mathbf{X}_{\mathtt{L}(P-Q)} \end{array}\right], \quad \mathbf{X}_{\mathtt{R}} = \left[\begin{array}{c} \mathbf{X}_{\mathtt{R}1} \\ \vdots \\ \mathbf{X}_{\mathtt{R}Q} \\ \hline \mathbf{X}_{\mathtt{R}(Q+1)} \\ \vdots \\ \mathbf{X}_{\mathtt{R}(P-Q)} \end{array}\right]. \tag{16}$$

Then, Eqs. (14) and (15) yield:

$$\left[\begin{array}{cc} \mathbf{K}_{\mathtt{L}(\mathtt{qq})} & \mathbf{K}_{\mathtt{L}(\mathtt{qX})} \\ \mathbf{K}_{\mathtt{L}(\mathtt{Xq})} & \mathbf{K}_{\mathtt{L}(\mathtt{XX})} \end{array}\right]\left[\begin{array}{c} \mathbf{q}_{\mathtt{L}} \\ \mathbf{X}_{\mathtt{L}} \end{array}\right] = \left[\begin{array}{c} \mathbf{F}_{\mathtt{L}} \\ \mathbf{0} \end{array}\right], \quad \left[\begin{array}{cc} \mathbf{K}_{\mathtt{R}(\mathtt{qq})} & \mathbf{K}_{\mathtt{R}(\mathtt{qX})} \\ \mathbf{K}_{\mathtt{R}(\mathtt{Xq})} & \mathbf{K}_{\mathtt{R}(\mathtt{XX})} \end{array}\right]\left[\begin{array}{c} \mathbf{q}_{\mathtt{R}} \\ \mathbf{X}_{\mathtt{R}} \end{array}\right] = \left[\begin{array}{c} \mathbf{F}_{\mathtt{R}} \\ \mathbf{0} \end{array}\right], \tag{17}$$

where

$$\begin{aligned}
\mathbf{K}_{\mathtt{L}(\mathtt{qq})} &= \mathbf{K}_{\mathtt{L}},\\
\mathbf{K}_{\mathtt{L}(\mathtt{qX})} &= \left[\ 2\mathtt{i}\omega\Re\left\{\left[\mathbf{R}_{\mathtt{L}(2)}\cdots\mathbf{R}_{\mathtt{L}(2Q)}\right]\right\} - 2\Re\left\{\left[\overline{p_{\mathtt{L}(2)}}\mathbf{R}_{\mathtt{L}(2)}\cdots\overline{p_{\mathtt{L}(2Q)}}\mathbf{R}_{\mathtt{L}(2Q)}\right]\right\} \mid \mathtt{i}\omega\left[\mathbf{R}_{\mathtt{L}(2Q+1)}\cdots\mathbf{R}_{\mathtt{L}P}\right]\ \right],\\
\mathbf{K}_{\mathtt{L}(\mathtt{Xq})} &= \left[\begin{array}{c} -\mathbb{1}_{Q\times 1}\otimes\mathbf{I}_n \\ \hline -\mathbb{1}_{(P-2Q)\times 1}\otimes\mathbf{I}_n \end{array}\right],\\
\mathbf{K}_{\mathtt{L}(\mathtt{XX})} &= \left[\begin{array}{c|c} \mathtt{blkdiag}\left\{\left(-\omega^2 - 2\mathtt{i}\omega\Re\{p_{\mathtt{L}(2k)}\} + |p_{\mathtt{L}(2k)}|^2\right)\mathbf{I}_n\right\}_{k=1}^{Q} & \mathbf{0} \\ \hline \mathbf{0} & \mathtt{blkdiag}\left\{(-\omega^2 - \mathtt{i}\omega p_{\mathtt{L}k})\mathbf{I}_n\right\}_{k=2Q+1}^{P} \end{array}\right],
\end{aligned} \tag{18}$$

and

$$\begin{aligned}
\mathbf{K}_{\mathtt{R}(\mathtt{qq})} &= \mathbf{K}_{\mathtt{R}},\\
\mathbf{K}_{\mathtt{R}(\mathtt{qX})} &= \left[\ 2\mathtt{i}\omega\Re\left\{\left[\mathbf{R}_{\mathtt{R}(2)}\cdots\mathbf{R}_{\mathtt{R}(2Q)}\right]\right\} - 2\Re\left\{\left[\overline{p_{\mathtt{R}(2)}}\mathbf{R}_{\mathtt{R}(2)}\cdots\overline{p_{\mathtt{R}(2Q)}}\mathbf{R}_{\mathtt{R}(2Q)}\right]\right\} \mid \mathtt{i}\omega\left[\mathbf{R}_{\mathtt{R}(2Q+1)}\cdots\mathbf{R}_{\mathtt{R}P}\right]\ \right],\\
\mathbf{K}_{\mathtt{R}(\mathtt{Xq})} &= \left[\begin{array}{c} -\mathbb{1}_{Q\times 1}\otimes\mathbf{I}_n \\ \hline -\mathbb{1}_{(P-2Q)\times 1}\otimes\mathbf{I}_n \end{array}\right],\\
\mathbf{K}_{\mathtt{R}(\mathtt{XX})} &= \left[\begin{array}{c|c} \mathtt{blkdiag}\left\{\left(-\omega^2 - 2\mathtt{i}\omega\Re\{p_{\mathtt{R}(2k)}\} + |p_{\mathtt{R}(2k)}|^2\right)\mathbf{I}_n\right\}_{k=1}^{Q} & \mathbf{0} \\ \hline \mathbf{0} & \mathtt{blkdiag}\left\{(-\omega^2 - \mathtt{i}\omega p_{\mathtt{R}k})\mathbf{I}_n\right\}_{k=2Q+1}^{P} \end{array}\right],
\end{aligned} \tag{19}$$

where $\otimes$ denotes the Kronecker product. The block components of the matrices occurring in Eqs. (18) and (19) represent polynomials of $\mathtt{i}\omega$ of orders 0, 1 or 2, which as such can be simply and quickly convert to the time domain (see hereafter).

2.4. Absorbing boundary conditions in the time domain

By separating the terms of identical powers of $\mathtt{i}\omega$ in Eq. (17), and by invoking the classical time-frequency transforms $\mathbf{q}(\omega) \to \mathbf{q}(t)$, $\mathtt{i}\omega\mathbf{q} \to \dot{\mathbf{q}}$, $-\omega^2\mathbf{q} \to \ddot{\mathbf{q}}$ and $\mathbf{X}(\omega) \to \mathbf{X}(t)$, $\mathtt{i}\omega\mathbf{X} \to \dot{\mathbf{X}}$, $-\omega^2\mathbf{X} \to \ddot{\mathbf{X}}$ (where dot and double-dot notations mean single and double time derivatives, respectively), this yields:

$$\mathbb{M}_{\mathtt{L}} \begin{bmatrix} \ddot{\mathbf{q}}_{\mathtt{L}} \\ \ddot{\mathbf{X}}_{\mathtt{L}} \end{bmatrix} + \mathbb{C}_{\mathtt{L}} \begin{bmatrix} \dot{\mathbf{q}}_{\mathtt{L}} \\ \dot{\mathbf{X}}_{\mathtt{L}} \end{bmatrix} + \mathbb{K}_{\mathtt{L}} \begin{bmatrix} \mathbf{q}_{\mathtt{L}} \\ \mathbf{X}_{\mathtt{L}} \end{bmatrix} = \begin{bmatrix} \mathbf{F}_{\mathtt{L}} \\ \mathbf{0} \end{bmatrix} \quad , \quad \mathbb{M}_{\mathtt{R}} \begin{bmatrix} \ddot{\mathbf{q}}_{\mathtt{R}} \\ \ddot{\mathbf{X}}_{\mathtt{R}} \end{bmatrix} + \mathbb{C}_{\mathtt{R}} \begin{bmatrix} \dot{\mathbf{q}}_{\mathtt{R}} \\ \dot{\mathbf{X}}_{\mathtt{R}} \end{bmatrix} + \mathbb{K}_{\mathtt{R}} \begin{bmatrix} \mathbf{q}_{\mathtt{R}} \\ \mathbf{X}_{\mathtt{R}} \end{bmatrix} = \begin{bmatrix} \mathbf{F}_{\mathtt{R}} \\ \mathbf{0} \end{bmatrix}, \tag{20}$$

where:

$$\mathbb{M}_{\mathtt{L}} = \left[\begin{array}{c|c|c} \mathbf{0} & \mathbf{0} & \mathbf{0} \\ \hline \mathbf{0} & \mathtt{blkdiag}\left\{\mathbf{I}_n\right\}_{k=1}^{Q} & \mathbf{0} \\ \hline \mathbf{0} & \mathbf{0} & \mathtt{blkdiag}\left\{\mathbf{I}_n\right\}_{k=2Q+1}^{P} \end{array}\right],$$

$$\mathbb{C}_{\mathtt{L}} = \left[\begin{array}{c|c|c} \mathbf{0} & 2\Re\left\{\left[\mathbf{R}_{\mathtt{L}(2)} \cdots \mathbf{R}_{\mathtt{L}(2Q)}\right]\right\} & \left[\mathbf{R}_{\mathtt{L}(2Q+1)} \cdots \mathbf{R}_{\mathtt{L}P}\right] \\ \hline \mathbf{0} & \mathtt{blkdiag}\left\{-2\Re\{p_{\mathtt{L}(2k)}\}\mathbf{I}_n\right\}_{k=1}^{Q} & \mathbf{0} \\ \hline \mathbf{0} & \mathbf{0} & \mathtt{blkdiag}\left\{-p_{\mathtt{L}k}\mathbf{I}_n\right\}_{k=2Q+1}^{P} \end{array}\right],$$

$$\mathbb{K}_{\mathtt{L}} = \left[\begin{array}{c|c|c} \mathbf{K}_{\mathtt{L}} & -2\Re\left\{\left[\overline{p_{\mathtt{L}(2)}}\mathbf{R}_{\mathtt{L}(2)} \cdots \overline{p_{\mathtt{L}(2Q)}}\mathbf{R}_{\mathtt{L}(2Q)}\right]\right\} & \mathbf{0} \\ \hline -\mathbb{1}_{Q\times 1} \otimes \mathbf{I}_n & \mathtt{blkdiag}\left\{|p_{\mathtt{L}(2k)}|^2\mathbf{I}_n\right\}_{k=1}^{Q} & \mathbf{0} \\ \hline -\mathbb{1}_{(P-2Q)\times 1} \otimes \mathbf{I}_n & \mathbf{0} & \mathbf{0} \end{array}\right], \tag{21}$$

and

$$\mathbb{M}_{\mathtt{R}} = \left[\begin{array}{c|c|c} \mathbf{0} & \mathbf{0} & \mathbf{0} \\ \hline \mathbf{0} & \mathtt{blkdiag}\left\{\mathbf{I}_n\right\}_{k=1}^{Q} & \mathbf{0} \\ \hline \mathbf{0} & \mathbf{0} & \mathtt{blkdiag}\left\{\mathbf{I}_n\right\}_{k=2Q+1}^{P} \end{array}\right],$$

$$\mathbb{C}_{\mathtt{R}} = \left[\begin{array}{c|c|c} \mathbf{0} & 2\Re\left\{\left[\mathbf{R}_{\mathtt{R}(2)} \cdots \mathbf{R}_{\mathtt{R}(2Q)}\right]\right\} & \left[\mathbf{R}_{\mathtt{R}(2Q+1)} \cdots \mathbf{R}_{\mathtt{R}P}\right] \\ \hline \mathbf{0} & \mathtt{blkdiag}\left\{-2\Re\{p_{\mathtt{R}(2k)}\}\mathbf{I}_n\right\}_{k=1}^{Q} & \mathbf{0} \\ \hline \mathbf{0} & \mathbf{0} & \mathtt{blkdiag}\left\{-p_{\mathtt{R}k}\mathbf{I}_n\right\}_{k=2Q+1}^{P} \end{array}\right],$$

$$\mathbb{K}_{\mathtt{R}} = \left[\begin{array}{c|c|c} \mathbf{K}_{\mathtt{R}} & -2\Re\left\{\left[\overline{p_{\mathtt{R}(2)}}\mathbf{R}_{\mathtt{R}(2)} \cdots \overline{p_{\mathtt{R}(2Q)}}\mathbf{R}_{\mathtt{R}(2Q)}\right]\right\} & \mathbf{0} \\ \hline -\mathbb{1}_{Q\times 1} \otimes \mathbf{I}_n & \mathtt{blkdiag}\left\{|p_{\mathtt{R}(2k)}|^2\mathbf{I}_n\right\}_{k=1}^{Q} & \mathbf{0} \\ \hline -\mathbb{1}_{(P-2Q)\times 1} \otimes \mathbf{I}_n & \mathbf{0} & \mathbf{0} \end{array}\right]. \tag{22}$$

Let us denote by $\mathbf{M}$, $\mathbf{C}$ and $\mathbf{K}$ the mass, damping and stiffness matrices of the periodic structure (N substructures), and let us write the related equation of motion as follows:

$$\mathbf{M}\ddot{\mathbf{q}} + \mathbf{C}\dot{\mathbf{q}} + \mathbf{K}\mathbf{q} = \mathbf{F}, \tag{23}$$

where $\mathbf{q} = \mathbf{q}(t)$ and $\mathbf{F} = \mathbf{F}(t)$ are the displacement and force vectors, respectively. In this case, the force vector is expressed by $\mathbf{F} = [\mathbf{F}_{\mathtt{I}}^T \mathbf{F}_{\mathtt{L}}^T \mathbf{F}_{\mathtt{R}}^T]$ where $\mathbf{F}_{\mathtt{L}}$ and $\mathbf{F}_{\mathtt{R}}$ refer to the force vectors on $S_{\mathtt{L}}$ and $S_{\mathtt{R}}$ (absorbing BCs), and $\mathbf{F}_{\mathtt{I}}$ refers to the force vector for the internal DOFs ($\mathtt{I}$) of the structure. Also, the displacement vector is expressed by $\mathbf{q} = [\mathbf{q}_{\mathtt{I}}^T \mathbf{q}_{\mathtt{L}}^T \mathbf{q}_{\mathtt{R}}^T]$ where $\mathbf{q}_{\mathtt{I}}$ is the displacement vector for the internal DOFs. Then, let us rewrite Eq. (23) as follows:

$$\begin{bmatrix} \mathbf{M}_{\mathtt{II}} & \mathbf{M}_{\mathtt{IL}} & \mathbf{M}_{\mathtt{IR}} \\ \mathbf{M}_{\mathtt{LI}} & \mathbf{M}_{\mathtt{LL}} & \mathbf{M}_{\mathtt{LR}} \\ \mathbf{M}_{\mathtt{RI}} & \mathbf{M}_{\mathtt{RL}} & \mathbf{M}_{\mathtt{RR}} \end{bmatrix} \begin{bmatrix} \ddot{\mathbf{q}}_{\mathtt{I}} \\ \ddot{\mathbf{q}}_{\mathtt{L}} \\ \ddot{\mathbf{q}}_{\mathtt{R}} \end{bmatrix} + \begin{bmatrix} \mathbf{C}_{\mathtt{II}} & \mathbf{C}_{\mathtt{IL}} & \mathbf{C}_{\mathtt{IR}} \\ \mathbf{C}_{\mathtt{LI}} & \mathbf{C}_{\mathtt{LL}} & \mathbf{C}_{\mathtt{LR}} \\ \mathbf{C}_{\mathtt{RI}} & \mathbf{C}_{\mathtt{RL}} & \mathbf{C}_{\mathtt{RR}} \end{bmatrix} \begin{bmatrix} \dot{\mathbf{q}}_{\mathtt{I}} \\ \dot{\mathbf{q}}_{\mathtt{L}} \\ \dot{\mathbf{q}}_{\mathtt{R}} \end{bmatrix} + \begin{bmatrix} \mathbf{K}_{\mathtt{II}} & \mathbf{K}_{\mathtt{IL}} & \mathbf{K}_{\mathtt{IR}} \\ \mathbf{K}_{\mathtt{LI}} & \mathbf{K}_{\mathtt{LL}} & \mathbf{K}_{\mathtt{LR}} \\ \mathbf{K}_{\mathtt{RI}} & \mathbf{K}_{\mathtt{RL}} & \mathbf{K}_{\mathtt{RR}} \end{bmatrix} \begin{bmatrix} \mathbf{q}_{\mathtt{I}} \\ \mathbf{q}_{\mathtt{L}} \\ \mathbf{q}_{\mathtt{R}} \end{bmatrix} = \begin{bmatrix} \mathbf{F}_{\mathtt{I}} \\ \mathbf{F}_{\mathtt{L}} \\ \mathbf{F}_{\mathtt{R}} \end{bmatrix}. \tag{24}$$

By considering the absorbing BCs (Eq. (20)), this yields:

$$\mathbf{M}_{\mathtt{tot}} \begin{bmatrix} \ddot{\mathbf{q}}_{\mathtt{I}} \\ \ddot{\mathbf{q}}_{\mathtt{L}} \\ \ddot{\mathbf{q}}_{\mathtt{R}} \\ \ddot{\mathbf{X}}_{\mathtt{L}} \\ \ddot{\mathbf{X}}_{\mathtt{R}} \end{bmatrix} + \mathbf{C}_{\mathtt{tot}} \begin{bmatrix} \dot{\mathbf{q}}_{\mathtt{I}} \\ \dot{\mathbf{q}}_{\mathtt{L}} \\ \dot{\mathbf{q}}_{\mathtt{R}} \\ \dot{\mathbf{X}}_{\mathtt{L}} \\ \dot{\mathbf{X}}_{\mathtt{R}} \end{bmatrix} + \mathbf{K}_{\mathtt{tot}} \begin{bmatrix} \mathbf{q}_{\mathtt{I}} \\ \mathbf{q}_{\mathtt{L}} \\ \mathbf{q}_{\mathtt{R}} \\ \mathbf{X}_{\mathtt{L}} \\ \mathbf{X}_{\mathtt{R}} \end{bmatrix} = \begin{bmatrix} \mathbf{F}_{\mathtt{I}} \\ \mathbf{0} \\ \mathbf{0} \\ \mathbf{0} \\ \mathbf{0} \end{bmatrix}. \tag{25}$$

Eq. (25) represents a second-order differential matrix equation for the displacement vector $\mathbf{q}$ and the vector of supplementary variables $\mathbf{X} = [\mathbf{X}_{\mathtt{L}}^T \mathbf{X}_{\mathtt{R}}^T]^T$. This indeed represents a classical dynamic equation, in the time domain, of a structure with absorbing BCs and subject to an input force vector $\mathbf{F}_{\mathtt{I}} = \mathbf{F}_{\mathtt{I}}(t)$, with the only modification that supplementary DOFs are added at the boundaries. Therefore, this equation can be solved in a standard way via a time integration numerical scheme (e.g., Newmark scheme).

In (25), the matrices $\mathbf{M}_{\mathtt{tot}}$, $\mathbf{C}_{\mathtt{tot}}$ and $\mathbf{K}_{\mathtt{tot}}$ are given by:

$$\mathbf{M}_{\mathtt{tot}} = \begin{bmatrix} \mathbf{M}_{\mathtt{II}} & \mathbf{M}_{\mathtt{IL}} & \mathbf{M}_{\mathtt{IR}} & \mathbf{0} & \mathbf{0} \\ \mathbf{M}_{\mathtt{LI}} & \mathbf{M}_{\mathtt{LL}} & \mathbf{M}_{\mathtt{LR}} & \mathbf{0} & \mathbf{0} \\ \mathbf{M}_{\mathtt{RI}} & \mathbf{M}_{\mathtt{RL}} & \mathbf{M}_{\mathtt{RR}} & \mathbf{0} & \mathbf{0} \\ \mathbf{0} & \mathbf{0} & \mathbf{0} & \mathbb{M}_{\mathtt{L(XX)}} & \mathbf{0} \\ \mathbf{0} & \mathbf{0} & \mathbf{0} & \mathbf{0} & \mathbb{M}_{\mathtt{R(XX)}} \end{bmatrix},$$

$$\mathbf{C}_{\mathtt{tot}} = \begin{bmatrix} \mathbf{C}_{\mathtt{II}} & \mathbf{C}_{\mathtt{IL}} & \mathbf{C}_{\mathtt{IR}} & \mathbf{0} & \mathbf{0} \\ \mathbf{C}_{\mathtt{LI}} & \mathbf{C}_{\mathtt{LL}} & \mathbf{C}_{\mathtt{LR}} & -\mathbb{C}_{\mathtt{L(qX)}} & \mathbf{0} \\ \mathbf{C}_{\mathtt{RI}} & \mathbf{C}_{\mathtt{RL}} & \mathbf{C}_{\mathtt{RR}} & \mathbf{0} & -\mathbb{C}_{\mathtt{R(qX)}} \\ \mathbf{0} & \mathbf{0} & \mathbf{0} & \mathbb{C}_{\mathtt{L(XX)}} & \mathbf{0} \\ \mathbf{0} & \mathbf{0} & \mathbf{0} & \mathbf{0} & \mathbb{C}_{\mathtt{R(XX)}} \end{bmatrix},$$

$$\mathbf{K}_{\mathtt{tot}} = \begin{bmatrix} \mathbf{K}_{\mathtt{II}} & \mathbf{K}_{\mathtt{IL}} & \mathbf{K}_{\mathtt{IR}} & \mathbf{0} & \mathbf{0} \\ \mathbf{K}_{\mathtt{LI}} & \mathbf{K}_{\mathtt{LL}} - \mathbb{K}_{\mathtt{L(qq)}} & \mathbf{K}_{\mathtt{LR}} & -\mathbb{K}_{\mathtt{L(qX)}} & \mathbf{0} \\ \mathbf{K}_{\mathtt{RI}} & \mathbf{K}_{\mathtt{RL}} & \mathbf{K}_{\mathtt{RR}} - \mathbb{K}_{\mathtt{R(qq)}} & \mathbf{0} & -\mathbb{K}_{\mathtt{R(qX)}} \\ \mathbf{0} & \mathbb{K}_{\mathtt{L(Xq)}} & \mathbf{0} & \mathbb{K}_{\mathtt{L(XX)}} & \mathbf{0} \\ \mathbf{0} & \mathbf{0} & \mathbb{K}_{\mathtt{R(Xq)}} & \mathbf{0} & \mathbb{K}_{\mathtt{R(XX)}} \end{bmatrix}, \tag{26}$$

where:

$$
\begin{aligned}
\mathbb{M}_{\mathtt{L(XX)}} &= \left[\begin{array}{c|c} \mathtt{blkdiag}\left\{\mathbf{I}_n\right\}_{k=1}^{Q} & \mathbf{0} \\ \hline \mathbf{0} & \mathtt{blkdiag}\left\{\mathbf{I}_n\right\}_{k=2Q+1}^{P} \end{array}\right], \\
\mathbb{C}_{\mathtt{L(qX)}} &= \left[\begin{array}{c|c} 2\Re\left\{\left[\mathbf{R}_{\mathtt{L}(2)} \cdots \mathbf{R}_{\mathtt{L}(2Q)}\right]\right\} & \left[\mathbf{R}_{\mathtt{L}(2Q+1)} \cdots \mathbf{R}_{\mathtt{L}N}\right] \end{array}\right], \\
\mathbb{C}_{\mathtt{L(XX)}} &= \left[\begin{array}{c|c} \mathtt{blkdiag}\left\{-2\Re\{p_{\mathtt{L}(2k)}\}\mathbf{I}_n\right\}_{k=1}^{Q} & \mathbf{0} \\ \hline \mathbf{0} & \mathtt{blkdiag}\left\{-p_{\mathtt{L}k}\mathbf{I}_n\right\}_{k=2Q+1}^{P} \end{array}\right], \\
\mathbb{K}_{\mathtt{L(qq)}} &= \mathbf{K}_{\mathtt{L}}, \\
\mathbb{K}_{\mathtt{L(qX)}} &= \left[\begin{array}{c|c} -2\Re\left\{\left[\overline{p_{\mathtt{L}(2)}}\mathbf{R}_{\mathtt{L}(2)} \cdots \overline{p_{\mathtt{L}(2Q)}}\mathbf{R}_{\mathtt{L}(2Q)}\right]\right\} & \mathbf{0} \end{array}\right], \\
\mathbb{K}_{\mathtt{L(Xq)}} &= \left[\begin{array}{c} -\mathbb{1}_{Q\times 1} \otimes \mathbf{I}_n \\ \hline -\mathbb{1}_{(P-2Q)\times 1} \otimes \mathbf{I}_n \end{array}\right], \\
\mathbb{K}_{\mathtt{L(XX)}} &= \left[\begin{array}{c|c} \mathtt{blkdiag}\left\{|p_{\mathtt{L}(2k)}|^2\mathbf{I}_n\right\}_{k=1}^{Q} & \mathbf{0} \\ \hline \mathbf{0} & \mathbf{0} \end{array}\right],
\end{aligned}
\tag{27}
$$

and

$$
\begin{aligned}
\mathbb{M}_{\mathtt{R(XX)}} &= \left[\begin{array}{c|c} \mathtt{blkdiag}\left\{\mathbf{I}_n\right\}_{k=1}^{Q} & \mathbf{0} \\ \hline \mathbf{0} & \mathtt{blkdiag}\left\{\mathbf{I}_n\right\}_{k=2Q+1}^{P} \end{array}\right], \\
\mathbb{C}_{\mathtt{R(qX)}} &= \left[\begin{array}{c|c} 2\Re\left\{\left[\mathbf{R}_{\mathtt{R}(2)} \cdots \mathbf{R}_{\mathtt{R}(2Q)}\right]\right\} & \left[\mathbf{R}_{\mathtt{R}(2Q+1)} \cdots \mathbf{R}_{\mathtt{R}N}\right] \end{array}\right], \\
\mathbb{C}_{\mathtt{R(XX)}} &= \left[\begin{array}{c|c} \mathtt{blkdiag}\left\{-2\Re\{p_{\mathtt{R}(2k)}\}\mathbf{I}_n\right\}_{k=1}^{Q} & \mathbf{0} \\ \hline \mathbf{0} & \mathtt{blkdiag}\left\{-p_{\mathtt{R}k}\mathbf{I}_n\right\}_{k=2Q+1}^{P} \end{array}\right], \\
\mathbb{K}_{\mathtt{R(qq)}} &= \mathbf{K}_{\mathtt{R}}, \\
\mathbb{K}_{\mathtt{R(qX)}} &= \left[\begin{array}{c|c} -2\Re\left\{\left[\overline{p_{\mathtt{R}(2)}}\mathbf{R}_{\mathtt{R}(2)} \cdots \overline{p_{\mathtt{R}(2Q)}}\mathbf{R}_{\mathtt{R}(2Q)}\right]\right\} & \mathbf{0} \end{array}\right], \\
\mathbb{K}_{\mathtt{R(Xq)}} &= \left[\begin{array}{c} -\mathbb{1}_{Q\times 1} \otimes \mathbf{I}_n \\ \hline -\mathbb{1}_{(P-2Q)\times 1} \otimes \mathbf{I}_n \end{array}\right], \\
\mathbb{K}_{\mathtt{R(XX)}} &= \left[\begin{array}{c|c} \mathtt{blkdiag}\left\{|p_{\mathtt{R}(2k)}|^2\mathbf{I}_n\right\}_{k=1}^{Q} & \mathbf{0} \\ \hline \mathbf{0} & \mathbf{0} \end{array}\right].
\end{aligned}
\tag{28}
$$

2.5. Solution by implicit methods

Let us rewrite Eq. (25) in concise form as follows:

$$
\mathbf{M}_{\mathtt{tot}}\ddot{\mathbf{y}} + \mathbf{C}_{\mathtt{tot}}\dot{\mathbf{y}} + \mathbf{K}_{\mathtt{tot}}\mathbf{y} = \mathbf{F}_{\mathtt{tot}}, \tag{29}
$$

where

$$
\mathbf{y} = \mathbf{y}(t) = \left[\begin{array}{c} \mathbf{q}_{\mathtt{I}}(t) \\ \mathbf{q}_{\mathtt{L}}(t) \\ \mathbf{q}_{\mathtt{R}}(t) \\ \mathbf{X}_{\mathtt{L}}(t) \\ \mathbf{X}_{\mathtt{R}}(t) \end{array}\right] \quad , \quad \mathbf{F}_{\mathtt{tot}} = \mathbf{F}_{\mathtt{tot}}(t) = \left[\begin{array}{c} \mathbf{F}_{\mathtt{I}}(t) \\ \mathbf{0} \\ \mathbf{0} \\ \mathbf{0} \\ \mathbf{0} \end{array}\right]. \tag{30}
$$

Eq. (29) can be solved by means of the classical Newmark algorithm. Hence, consider a time step of Δt and define the following vector $\mathbf{y}^n = \mathbf{y}(n\Delta t)$ which represents the vector $\mathbf{y}$ expressed at a discrete time $n\Delta t$ for $n = 0, 1, 2, \ldots$. Following the Newmark scheme, one has:

$$\begin{aligned} \mathbf{y}^{n+1} &= \tilde{\mathbf{y}}^{n+1} + \beta\Delta t^2 \ddot{\mathbf{y}}^{n+1}, \\ \dot{\mathbf{y}}^{n+1} &= \tilde{\dot{\mathbf{y}}}^{n+1} + \gamma\Delta t \ddot{\mathbf{y}}^{n+1}, \end{aligned} \tag{31}$$

where

$$\begin{aligned} \tilde{\mathbf{y}}^{n+1} &= \mathbf{y}^n + \Delta t \dot{\mathbf{y}}^n + (\frac{1}{2} - \beta)\Delta t^2 \ddot{\mathbf{y}}^n, \\ \tilde{\dot{\mathbf{y}}}^{n+1} &= \dot{\mathbf{y}}^n + (1-\gamma)\Delta t \ddot{\mathbf{y}}^n, \end{aligned} \tag{32}$$

and

$$\ddot{\mathbf{y}}^{n+1} = \frac{1}{\beta\Delta t^2}(\mathbf{y}^{n+1} - \tilde{\mathbf{y}}^{n+1}). \tag{33}$$

Also, in Eq. (31), γ and β are the so-called Newmark parameters, e.g., $\gamma = 1/2$ and $\beta = 1/4$ (average constant acceleration rule). The residue of relation (29) is given by:

$$\mathbf{r}(\mathbf{y}) = \mathbf{M}_{\mathtt{tot}}\ddot{\mathbf{y}} + \mathbf{C}_{\mathtt{tot}}\dot{\mathbf{y}} + \mathbf{K}_{\mathtt{tot}}\mathbf{y} - \mathbf{F}_{\mathtt{tot}}. \tag{34}$$

From the knowledge of the solution at $n\Delta t$, one has to find the solution at the subsequent time $(n+1)\Delta t$ such that:

$$\begin{aligned} \mathbf{r}(\mathbf{y}^{n+1}) &= \mathbf{M}_{\mathtt{tot}}\ddot{\mathbf{y}}^{n+1} + \mathbf{C}_{\mathtt{tot}}\dot{\mathbf{y}}^{n+1} + \mathbf{K}_{\mathtt{tot}}\mathbf{y}^{n+1} - \mathbf{F}_{\mathtt{tot}}(t_{n+1}) \\ &= \frac{1}{\beta\Delta t^2}\mathbf{M}_{\mathtt{tot}}(\mathbf{y}^{n+1} - \tilde{\mathbf{y}}^{n+1}) + \mathbf{C}_{\mathtt{tot}}(\tilde{\dot{\mathbf{y}}}^{n+1} + \frac{\gamma}{\beta\Delta t}(\mathbf{y}^{n+1} - \tilde{\mathbf{y}}^{n+1})) \\ &\quad + \mathbf{K}_{\mathtt{tot}}\mathbf{y}^{n+1} - \mathbf{F}_{\mathtt{tot}}(t_{n+1}) \\ &= \mathbf{0}. \end{aligned} \tag{35}$$

The solution at $(n+1)\Delta t$ follows by solving a linear system:

$$\tilde{\mathbf{M}}\mathbf{y}^{n+1} = \mathbf{F}^{n+1}, \tag{36}$$

where:

$$\begin{aligned} \tilde{\mathbf{M}} &= \frac{1}{\beta\Delta t^2}\mathbf{M}_{\mathtt{tot}} + \frac{\gamma}{\beta\Delta t}\mathbf{C}_{\mathtt{tot}} + \mathbf{K}_{\mathtt{tot}}, \\ \mathbf{F}^{n+1} &= \frac{1}{\beta\Delta t^2}\mathbf{M}_{\mathtt{tot}}\tilde{\mathbf{y}}^{n+1} - \mathbf{C}_{\mathtt{tot}}(\tilde{\dot{\mathbf{y}}}^{n+1} - \frac{\gamma}{\beta\Delta t}\tilde{\mathbf{y}}^{n+1}) + \mathbf{F}_{\mathtt{tot}}(t_{n+1}). \end{aligned} \tag{37}$$

3. Euler-Bernoulli beam on an elastic foundation

For validation purposes, let us analyze the dynamic response of an infinite Euler-Bernoulli beam lying on an elastic foundation (lineic stiffness $k_{\mathtt{f}}$) as shown in Fig. 3 and subject to some "localized" lineic forces $f(x,t)$ for which analytical solutions are available. In this case, the governing equation of motion of the beam is given by:

$$\rho S\ddot{v} + EI\left(\frac{\partial^4 v}{\partial x^4} + \xi\frac{\partial^4 \dot{v}}{\partial x^4}\right) + k_{\mathtt{f}} v = f(x,t), \tag{38}$$

where $v = v(x,t)$ represents the transverse displacement, ρ is the density, S is the cross-sectional area, E is the Young's modulus, I is the inertia moment, and ξ is a damping parameter. For harmonic disturbance of the form $f(x)e^{\mathtt{i}\omega t}$, Eq. (38) leads to:

$$(-\rho S\omega^2 + k_{\mathtt{f}})v + EI(1+\mathtt{i}\omega\xi)\frac{\partial^4 v}{\partial x^4} = f(x), \tag{39}$$

where $v = v(x)$.

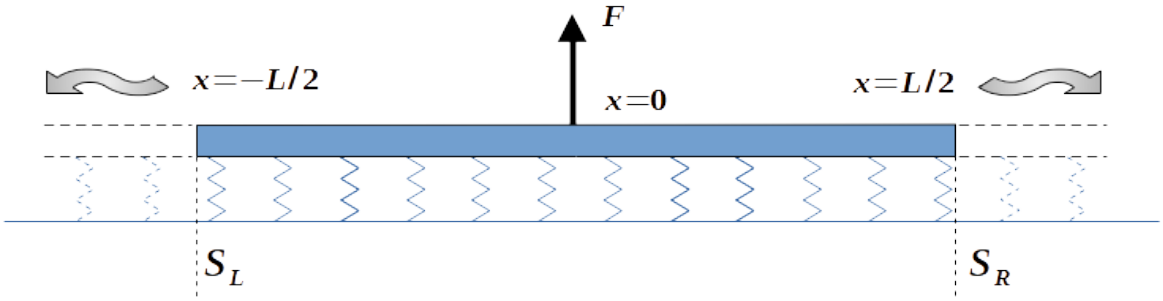

Figure 3: Infinite flexural beam on an elastic foundation.

This simple example of a beam on an elastic foundation aims at illustrating the methodology for obtaining absorbing BCs in time. There exist plenty of works about the dynamic analysis of beams with or without elastic foundations. However, even in this simple case, obtaining time absorbing BCs is not obvious. In fact, only a few works have been conducted on this topic. These mostly address approximate (not exact) expressions of absorbing BCs for Euler-Bernoulli beams. For instance, approximate expressions of absorbing BCs in time for Euler-Bernoulli beams have been proposed in [52]. In this case, the off-diagonal terms of the boundary impedance matrices are ignored, i.e., the coupling terms between the displacement and the moment and between the force and the rotation. Also, approximate expressions of absorbing BCs (in time) for beams under moving loads in convected coordinates have been proposed in [53]. In this case, absorbing BCs are obtained via the use of added stiffness and damping, tuned at a specific frequency. In [54], absorbing BCs have been derived for beams discretized by finite difference schemes. In [55], integrodifferential operators have been used for boundary dynamic feedback control to get absorbing BCs. In [56], artificial absorbing BCs in time have been proposed, while in [57], the PML method has been used. Finally, in [43], absorbing BCs for beams lying on a Winkler foundation have been obtained via the use of rational approximations for low frequencies, and asymptotic analysis and fractional derivatives for high frequencies. In this case, the proposed rational approximations appear to be roughly similar to those investigated in the present paper, except that in the present paper, the proposed approach is intended to work for complex periodic structures (not only for beams) and is not restricted to any low frequency assumptions other than those raised by the FE modeling.

3.1. Wave shapes: analytical expressions

For this simple case, there exist analytical expressions of the matrices of wave shapes $\mathbf{\Phi}_{\mathtt{q}}$, $\mathbf{\Phi}^{\star}_{\mathtt{q}}$, $\mathbf{\Phi}_{\mathtt{F}}$ and $\mathbf{\Phi}^{\star}_{\mathtt{F}}$, see Eq. (6). Here, the number of boundary DOFs is $n = 2$. The determination of these matrices involves solving Eq. (39) with $f(x) = 0$ (free wave propagation), which yields $v = Q_1 e^{-\mathtt{i}kx} + Q_2 e^{-kx} + Q_1^{\star} e^{\mathtt{i}kx} + Q_2^{\star} e^{kx}$ where:

$$k = \left(\frac{\rho S\omega^2 - k_{\mathtt{f}}}{EI(1+\mathtt{i}\omega\xi)}\right)^{1/4}. \tag{40}$$

Hence, by expressing the transverse displacement v together with the rotation $\theta = \partial v/\partial x$, this yields:

$$\begin{bmatrix} v \\ \theta \end{bmatrix} = \mathbf{\Phi}_{\mathtt{q}} \begin{bmatrix} e^{-\mathtt{i}kx} & 0 \\ 0 & e^{-kx} \end{bmatrix} \begin{bmatrix} Q_1 \\ Q_2 \end{bmatrix} + \mathbf{\Phi}^{\star}_{\mathtt{q}} \begin{bmatrix} e^{\mathtt{i}kx} & 0 \\ 0 & e^{kx} \end{bmatrix} \begin{bmatrix} Q^{\star}_1 \\ Q^{\star}_2 \end{bmatrix}, \tag{41}$$

where:

$$\mathbf{\Phi}_{\mathtt{q}} = \begin{bmatrix} 1 & 1 \\ -\mathtt{i}k & -k \end{bmatrix} \quad , \quad \mathbf{\Phi}^{\star}_{\mathtt{q}} = \begin{bmatrix} 1 & 1 \\ \mathtt{i}k & k \end{bmatrix}. \tag{42}$$

Also, by expressing the shearing force $V = -EI(\partial^3 v/\partial x^3)$ and the bending moment $M = EI(\partial^2 v/\partial x^2)$, this yields:

$$\begin{bmatrix} V \\ M \end{bmatrix} = \mathbf{\Phi}_{\mathtt{F}} \begin{bmatrix} e^{-\mathtt{i}kx} & 0 \\ 0 & e^{-kx} \end{bmatrix} \begin{bmatrix} Q_1 \\ Q_2 \end{bmatrix} + \mathbf{\Phi}^{\star}_{\mathtt{F}} \begin{bmatrix} e^{\mathtt{i}kx} & 0 \\ 0 & e^{kx} \end{bmatrix} \begin{bmatrix} Q^{\star}_1 \\ Q^{\star}_2 \end{bmatrix}, \tag{43}$$

where:

$$\mathbf{\Phi}_{\mathtt{F}} = EIk^2 \begin{bmatrix} -\mathtt{i}k & k \\ -1 & 1 \end{bmatrix} \quad , \quad \mathbf{\Phi}^{\star}_{\mathtt{F}} = EIk^2 \begin{bmatrix} \mathtt{i}k & -k \\ -1 & 1 \end{bmatrix}. \tag{44}$$

3.2. Impedance matrices: analytical expressions

Analytical expressions of the impedance matrices follow as $\mathbf{Z}_{\mathtt{L}} = -\mathbf{\Phi}^{\star}_{\mathtt{F}}(\mathbf{\Phi}^{\star}_{\mathtt{q}})^{-1}$ and $\mathbf{Z}_{\mathtt{R}} = \mathbf{\Phi}_{\mathtt{F}}(\mathbf{\Phi}_{\mathtt{q}})^{-1}$, see Eq. (10). In the present case, the matrix inverses $(\mathbf{\Phi}^{\star}_{\mathtt{q}})^{-1}$ and $(\mathbf{\Phi}_{\mathtt{q}})^{-1}$ are expressed by:

$$(\mathbf{\Phi}^{\star}_{\mathtt{q}})^{-1} = \frac{1}{1-\mathtt{i}} \begin{bmatrix} 1 & -\frac{1}{k} \\ -\mathtt{i} & \frac{1}{k} \end{bmatrix} \quad , \quad (\mathbf{\Phi}_{\mathtt{q}})^{-1} = \frac{1}{1-\mathtt{i}} \begin{bmatrix} 1 & \frac{1}{k} \\ -\mathtt{i} & -\frac{1}{k} \end{bmatrix}. \tag{45}$$

Therefore, the impedance matrices are written as:

$$\mathbf{Z}_{\mathtt{L}} = -\mathbf{\Phi}^{\star}_{\mathtt{F}}(\mathbf{\Phi}^{\star}_{\mathtt{q}})^{-1} = -\frac{EIk^2}{1-\mathtt{i}} \begin{bmatrix} 2\mathtt{i}k & -(1+\mathtt{i}) \\ -(1+\mathtt{i}) & \frac{2}{k} \end{bmatrix}, \tag{46}$$

and

$$\mathbf{Z}_{\mathtt{R}} = \mathbf{\Phi}_{\mathtt{F}}(\mathbf{\Phi}_{\mathtt{q}})^{-1} = -\frac{EIk^2}{1-\mathtt{i}} \begin{bmatrix} 2\mathtt{i}k & 1+\mathtt{i} \\ 1+\mathtt{i} & \frac{2}{k} \end{bmatrix}. \tag{47}$$

These are analytical expressions of the impedance matrices that could also have been obtained numerically by means of the WFE method. For more complex structures (see next section), only those obtained with the WFE method will be available.

3.3. Numerical results

Consider an infinite beam of rectangular cross-section having the following parameters: height $h = 0.001$ m, width $b = 0.01$ m (i.e., $S = bh$ and $I = bh^3/12$), Young's modulus $E = 2.2 \times 10^{11}$ Pa, density $\rho = 7800$ kg/m^3, damping parameter $\xi = 0.001$ s. Also, the lineic stiffness of the elastic foundation is $k_{\mathtt{f}} = 1$ N/m^2. The system is at rest at time $t = 0$ — i.e., $v(x,0) = 0$ and $\dot{v}(x,0) = 0$ — and, for $t \geq 0$, it is excited by a point harmonic force of frequency $f_0 = 5$ Hz (at $x = 0$):

$$f(x,t) = \cos(2\pi f_0 t)\delta(x) \qquad \text{for } t \geq 0. \tag{48}$$

The harmonic solution of this equation is found by solving Eq. (39) analytically, i.e.,

$$v(x,t) = \Re\left\{ \left(-\frac{\mathtt{i}}{4k_0^3 E_0 I} e^{-\mathtt{i}k_0|x|} - \frac{1}{4k_0^3 E_0 I} e^{-k_0|x|} \right) e^{\mathtt{i}\omega_0 t} \right\}, \tag{49}$$

which should match the solution of the equation of motion (38) after a certain time, i.e., once the transient effects become negligible. Here, the wavenumber k_0 is given by Eq. (40) when $\omega = \omega_0$; also, $E_0 = E(1 + \mathtt{i}\xi\omega_0)$.

On the other hand, the time-space response of the beam can be computed by considering the proposed approach. Within this framework, a beam of finite length L — i.e., $x \in [-L/2, L/2]$ where, for instance, $L = 5$ m — excited at $x = 0$ (Eq. (48)) is considered as shown in Fig. 3. Here, the system beam-foundation is modeled by means of 500 identical substructures that represent identical two-node Hermitian beam elements of length $d = 0.01$ m. For $f_0 = 5$ Hz, this gives a wavelength of $\lambda = 2\pi/\Re\{k_0\} = 0.39$ m and, therefore, 39 elements per wavelength. Additional numerical tests (not presented here) with $d = 0.1$ m and 4 elements per wavelength also give correct, although less accurate, results. As for the left and right boundaries $x = -L/2$ ($S_{\mathtt{L}}$) and $x = L/2$ ($S_{\mathtt{R}}$), they are described via absorbing BCs, see Secs. 2.3 and 2.4. The rational approximations of the impedance matrices $\mathbf{Z}_{\mathtt{L}}$ and $\mathbf{Z}_{\mathtt{R}}$ with P poles/residues (see Eqs. (11)) are computed with the MATLAB's rationalfit function. Especially, the components of the impedance matrix $\mathbf{Z}_{\mathtt{R}}$ issued from different orders P are plotted and compared to the analytical expressions given by Eq. (47) as shown in Fig. 4. Results show stable curves which closely match the analytical solutions for orders larger than $P = 7$. Besides, the relative errors between the proposed and analytical curves are given in Table 1 for orders up to $P = 12$ which is the value proposed by MATLAB and which will be used hereafter. ~~In this case, the relative error is smaller than −80 dB, which appears to be enough to meet good convergence.~~ The relative error e_{lm} on the lm component of the impedance matrix is defined as:

$$e_{lm} = \frac{(\sum_i |Z_{lm}^{\mathtt{rat}}(\omega_i) - Z_{lm}(\omega_i)|^2)^{1/2}}{(\sum_i |Z_{lm}(\omega_i)|^2)^{1/2}}, \tag{50}$$

with $Z_{lm}(\omega_i)$ the lm component of the impedance matrix at the discrete circular frequency ω_i, and $Z_{lm}^{\mathtt{rat}}(\omega_i)$ its rational approximation.

Table 1: Relative errors between the proposed and analytical solutions (components of the impedance matrix $\mathbf{Z}_{\mathtt{R}}$) for different orders P.

	Relative error			
Order P	3	7	10	12
Component (1,1)	0.261	0.011	5.46×10^{-4}	2.88×10^{-5}
Component (1,2)	0.106	4.51×10^{-3}	2.54×10^{-4}	6.83×10^{-6}
Component (2,2)	0.082	6.90×10^{-3}	5.49×10^{-4}	3.47×10^{-6}

Also, the transverse displacement of the beam can be computed. This involves solving the differential matrix equation (29) with the Newmark algorithm where $\Delta t = 0.01$ s, $\mathbf{y}^0 = \mathbf{0}$ and $\dot{\mathbf{y}}^0 = \mathbf{0}$. The related transverse displacement field, at $t = 4$ s and $t = 20$ s, are shown in Fig. 5 along with the analytical harmonic solution, Eq. (39). At time $t = 4$ s, the proposed and analytical solutions appear to be slightly different which is explained since transient effects are taken into account in the proposed solution, while they are not described with the analytical solution. Those transient effects become negligible after a certain time, e.g., $t = 20$ s as shown in Fig. 5. In this case, the proposed solution closely matches the analytical one, as expected.

Finally, Fig. 6 shows the history of the displacement solution at position $x = L/2$. Again, it is seen that, after a certain time (transient period), the solution issued from the proposed approach stabilizes towards the harmonic solution. Fig. 7 presents identical results in term of velocity where the proposed solution shows better accuracy than the displacement solution. Similar trends can be found for the acceleration (not displayed here).

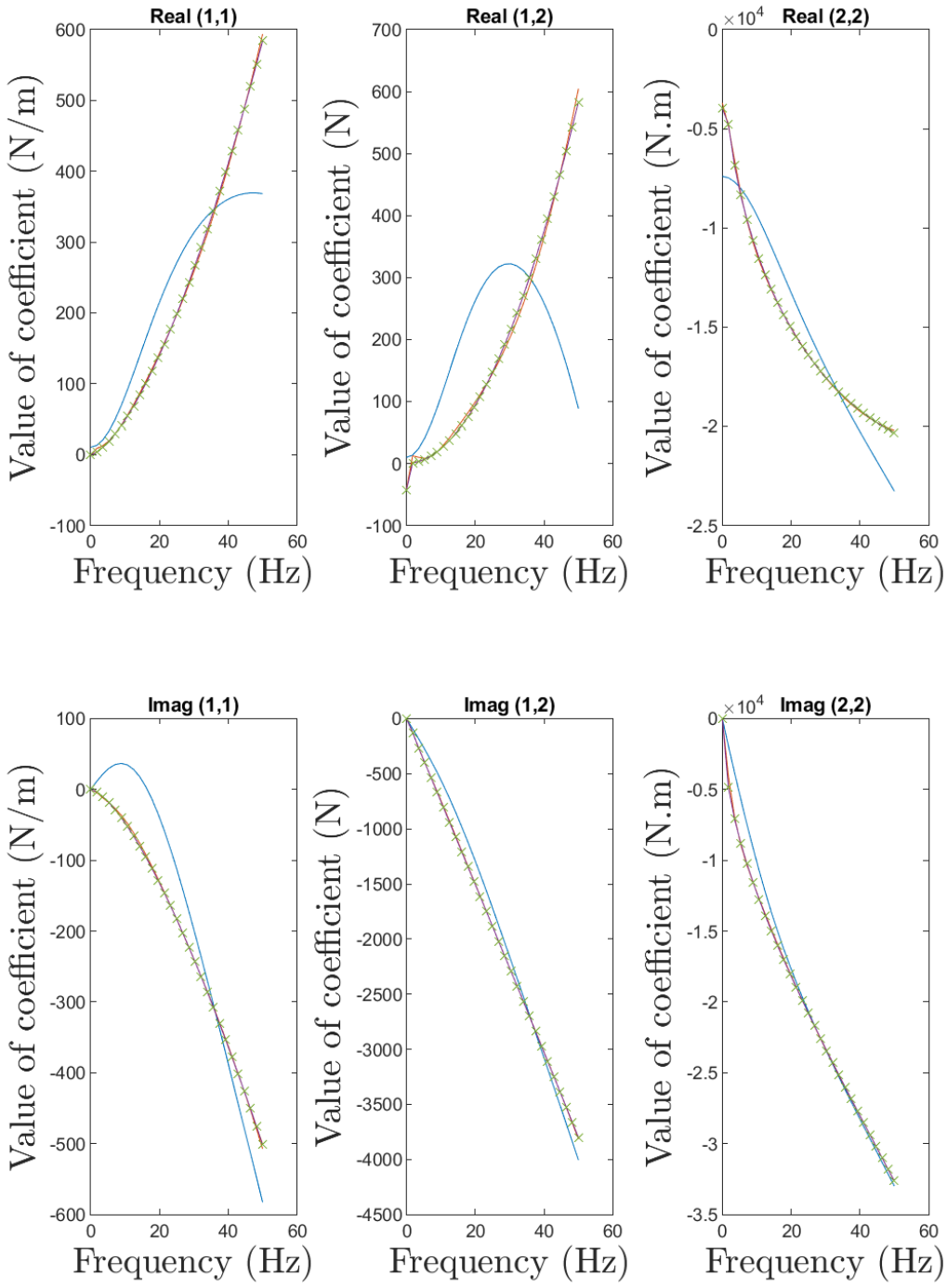

Figure 4: Real and imaginary parts of the components of the impedance matrix $\mathbf{Z}_{\mathrm{R}}$: (green crosses) Analytical solutions; (blue line) proposed solutions with $P = 3$; (red line) proposed solutions with $P = 7$; (orange line) proposed solutions with $P = 10$; (purple line) proposed solutions with $P = 12$.

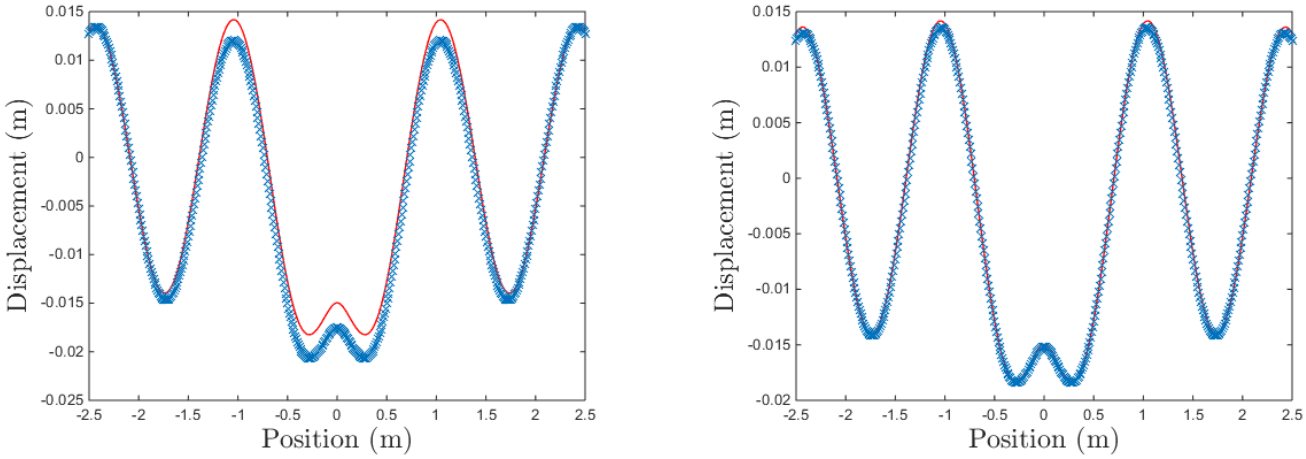

Figure 5: Transverse displacement field of the beam on the elastic foundation at $t = 4$ s (left) and $t = 20$ s (right): (blue crosses) Proposed approach; (red line) analytical harmonic solution.

Note that the proposed displacement solution is characterized by low frequency "ripples" (Fig. 6, left side) which are, however, less pronounced for the velocity solution. These correspond to transient phenomena of low frequencies generated by the initial conditions — i.e., the nullity of the displacement and the velocity at $t = 0$ s — which make the proposed solution far from the harmonic solution. The authors were able to verify through additional simulations that these ripples can be decreased by adding viscosity, e.g., by increasing ξ or by adding viscosity on the term $k_{\mathfrak{t}}$. More generally, these ripples are decreasing over time as this could be observed on an interval of $[0\,,\,40]$ s (not reproduced here).

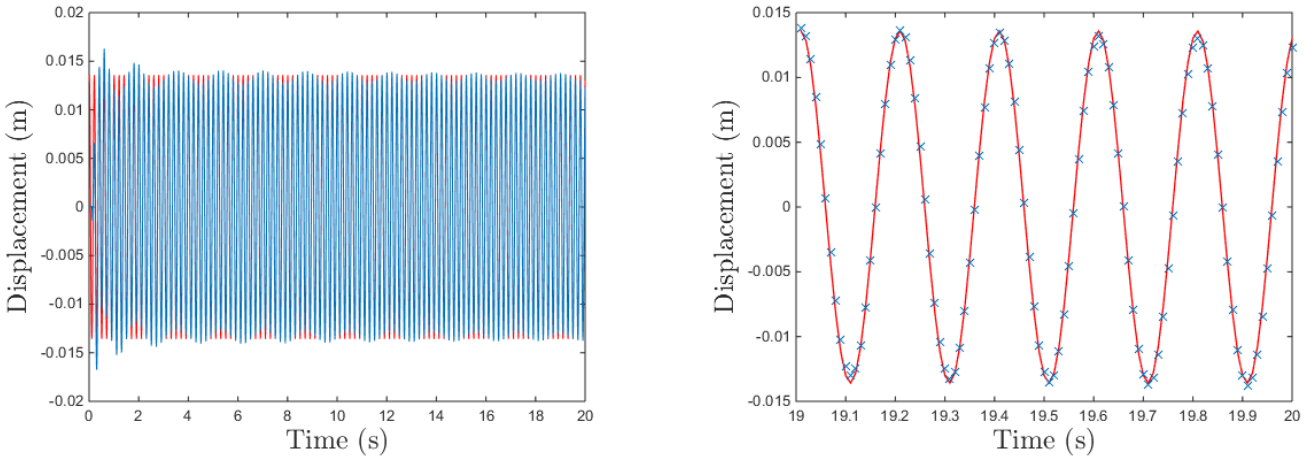

Figure 6: Time response at $x = L/2$ for $t \in [0\,,\,20]$ s (left) and $t \in [19\,,\,20]$ s (right). (blue line and crosses) Proposed approach; (red line) analytical theory, harmonic response.

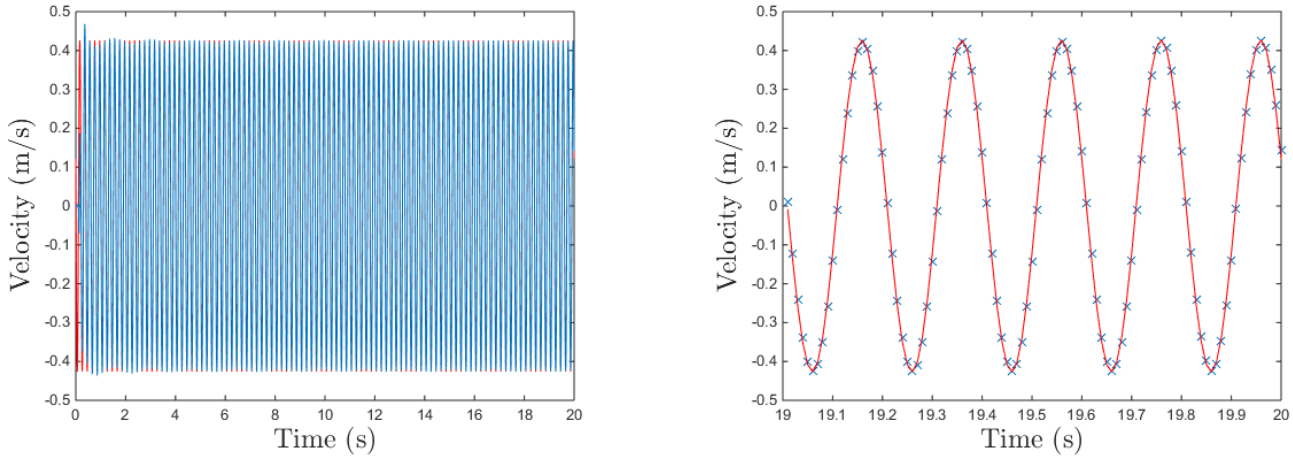

Figure 7: Time response of the velocity at $x = L/2$ for $t \in [0\,,\,20]$ s (left) and $t \in [19\,,\,20]$ s (right). (blue line and crosses) Proposed approach; (red line) analytical theory, harmonic response.

4. Periodic structure with 2D substructures

4.1. Square substructures with holes

Periodic structures are usually made up of substructures of complex shapes, which as such cannot be modeled analytically. Such periodic structures may concern, for instance, a 2D beam with periodic distributions of holes and elastic supports (springs of stiffness $K_{\mathtt{s}}$) as shown in Fig. 8. Here, square substructures of dimensions 2×2 m^2 with holes of radius 0.4 m are considered which are similar to those depicted in Fig. 2. The FE mesh of a substructure is generated on MATLAB with the DistMesh algorithm [58], and involves 2D linear plane stress triangular elements (three nodes) with $n = 26$ DOFs on the left and right boundaries. Regarding the modeling of the periodic supports, a nodal stiffness of $K_{\mathtt{s}}/2$ (vertical direction) is added to the FE model of the substructures at the left and right boundaries (bottom node). Other substructure parameters are: thickness $e = 0.005$ m, Young's modulus $E = 7 \times 10^{10}$ Pa, Poisson's ratio $\nu = 0.35$, density $\rho = 2700$ kg/m^3, and stiffness $K_{\mathtt{s}} = 10^5$ N/m. Rayleigh-type damping matrices $\mathbf{C}^s = a\mathbf{M}^s + b\mathbf{K}^s$ (see Sec. 2.2) are also considered where $a = 0.01$ s^{-1} and $b = 5 \times 10^{-5}$ s.

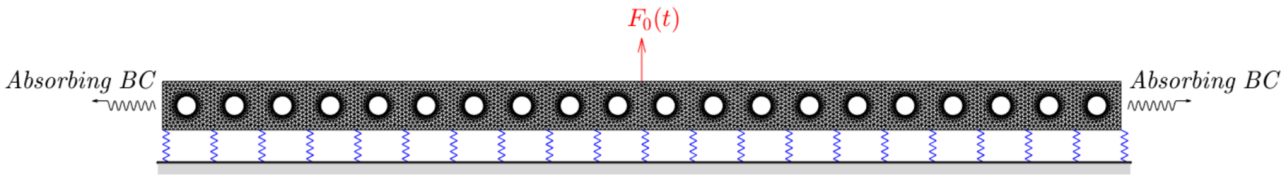

Figure 8: Schematic of an infinite periodic structure (square substructures with holes) with periodic elastic supports.

The time response of the infinite periodic structure subject to a vertical point force $F_0(t)$ at $x = 0$ (top node) is analyzed. Two kinds of excitations are considered, i.e., a harmonic force and a Ricker wavelet of frequency 100 Hz. Within the framework of the proposed approach, a periodic structure involving $N = 20$ substructures and absorbing BCs is considered as shown in Fig. 8. In this case, the structure has a length of $L = 40$ m and is supposed to be long enough to gather useful information about the local/evanescent displacement field in the vicinity of the excitation. The related FE model has been detailed in Secs. 2.3 and 2.4. In this case, the rational approximations of the impedance matrices $\mathbf{Z}_{\mathtt{L}}$ and $\mathbf{Z}_{\mathtt{R}}$ (Eq. (11)) are expressed by means of $P = 15$ poles/residues. The time response of the structure is computed over a time range of $[0\,,\,0.1]$ s by solving the differential matrix equation

(29) with the Newmark algorithm where $\Delta t = 10^{-4}$ s, $\mathbf{y}^0 = \mathbf{0}$ and $\dot{\mathbf{y}}^0 = \mathbf{0}$. For comparison purposes, an equivalent FE model of an "infinite" structure with a larger number of substructures (200) is considered and simulated over the time range $[0\,,\,0.1]$ s which is supposed to be small enough to prevent wave reflections (free boundaries).

4.1.1. Harmonic force

Consider a harmonic point force of magnitude $F_0(t) = 10^4 \cos(2\pi \times 100t)$ acting at $x = 0$, and assume that the structure is at rest at $t = 0$. The time response is analyzed over a time range of $[0\,,\,0.1]$ s which is supposed to be broad enough to include several oscillations (10 in this case) and cover the transient phase. Especially, the time variation of the transverse displacement at $x = 20$ m (right boundary, top node) can be computed as shown in Fig. 9. It is shown that the proposed solution perfectly matches the reference one over the whole time range. It is also numerically stable, i.e., a smooth curve that well predicts the oscillating nature of the signal.

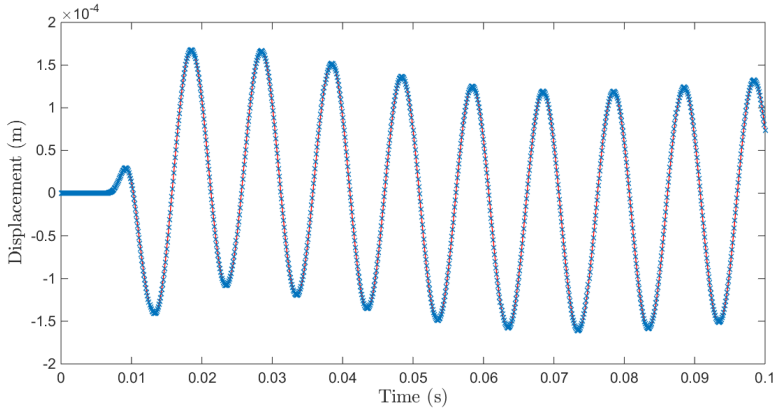

Figure 9: Periodic structure (square substructures with holes) subject to a harmonic force: time response at $x = L/2$ (top node, vertical displacement). (blue crosses) Proposed approach; (red line) reference FE method.

Additional simulations are made which concern the deformed shape of the structure at $t = 0.1$ s, where a scaling factor of 5×10^3 is used to magnify the displacement levels for a better understanding (see Fig. 10). Again, results show that the proposed solution is in perfect agreement with the reference one, which gives credit to the present work.

To further assess the accuracy of the proposed approach, the following relative error based on the displacement vector of the periodic structure (central part with 20 substructures) is investigated:

$$\mathtt{err} = \frac{\max\limits_n \|\mathbf{q}(t_n) - \mathbf{q}^{\mathtt{FE}}(t_n)\|_2}{\max\limits_n \|\mathbf{q}^{\mathtt{FE}}(t_n)\|_2}, \tag{51}$$

where $\mathbf{q} = [\mathbf{q}_{\mathtt{I}}^T \mathbf{q}_{\mathtt{L}}^T \mathbf{q}_{\mathtt{R}}^T]^T$ and $\mathbf{q}^{\mathtt{FE}} = [(\mathbf{q}_{\mathtt{I}}^{\mathtt{FE}})^T (\mathbf{q}_{\mathtt{L}}^{\mathtt{FE}})^T (\mathbf{q}_{\mathtt{R}}^{\mathtt{FE}})^T]^T$ are the displacement vectors of the periodic structure computed with the proposed approach and the FE method, respectively. Also, $\|\bullet\|_2$ denotes the 2−norm. More precisely, the proposed relative error $\mathtt{err}$ is defined as the ratio between the maximum error $\|\mathbf{q}(t_n) - \mathbf{q}^{\mathtt{FE}}(t_n)\|_2$ (among all the discrete times t_n considered) and the maximum value of $\|\mathbf{q}^{\mathtt{FE}}(t_n)\|_2$ (for the same discrete times). In the present case, this relative error yields $\mathtt{err} = 1.07\%$ which, therefore, validates the proposed approach.

4.1.2. Ricker wavelet force pulse

Consider now a Ricker wavelet, which might represent some shock applied to the structure at $x = 0$:

$$F_0(t) = 10^4 \times \left[1 - 2\pi^2 f_0^2 (t - t_0)^2\right] e^{-\pi^2 f_0^2 (t-t_0)^2} \qquad \text{for } t \geq 0, \tag{52}$$

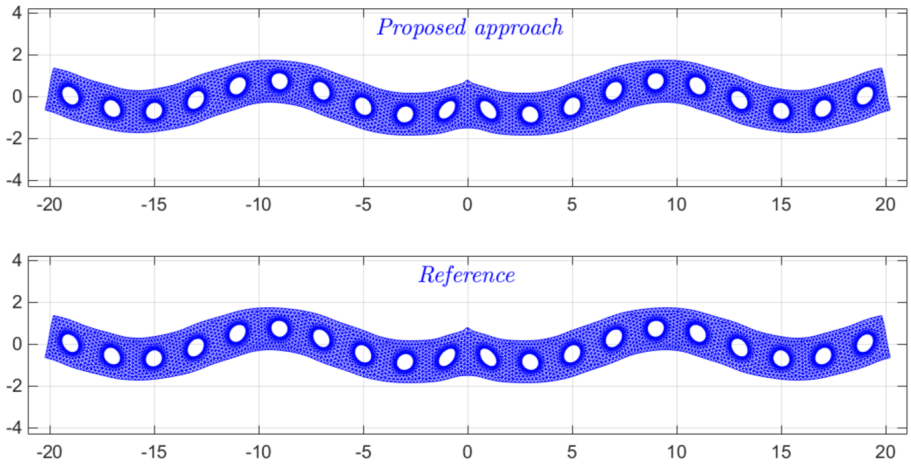

Figure 10: Periodic structure (square substructures with holes) subject to a harmonic force: deformed shape at $t = 0.1$ s.

where $f_0 = 100$ Hz and $t_0 = 5 \times 10^{-3}$ s. Again, the time history of the structure at $x = 20$ m can be computed as shown in Fig. (11). In this case again, the proposed solution appears to be numerically stable and in perfect agreement with the reference FE solution. A good match between those solutions is also observed regarding the deformed shapes of the structure, e.g., at $t = 0.01$ s as shown in Fig. 12. Also, the relative error made for computing the displacement vector of the periodic structure with the proposed approach can be assessed via Eq. (51), which gives $\texttt{err} = 1.05\%$. This completely validates the proposed approach.

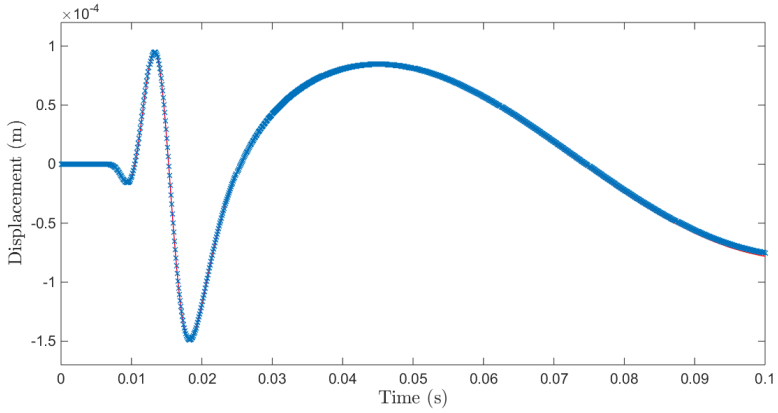

Figure 11: Periodic structure (square substructures with holes) subject to a Ricker wavelet pulse: time response at $x = L/2$ (top node, vertical displacement). (blue crosses) Proposed approach; (red line) reference FE method.

4.2. Square substructures with circular rubber layers

To further highlight the relevance of the proposed approach, a second test case is considered which concerns a periodic structure made up of square substructures with circular rubber layers, as shown in Fig. 13. The material properties of the inner parts (cores) and outer parts of the substructures — i.e., inside and outside the rubber layers — are similar to those depicted in Sec. 4.1. As for the rubber layers, the properties are: inner and outer radii of 0.3 m and 0.7 m, Young's modulus of 1.5×10^8 Pa, Poisson's ratio of 0.48 and density of 950 kg/m^3. The FE mesh of a substructure is shown in Fig. 13 and involves 2D linear plane stress triangular elements with $n = 42$ DOFs on the left and

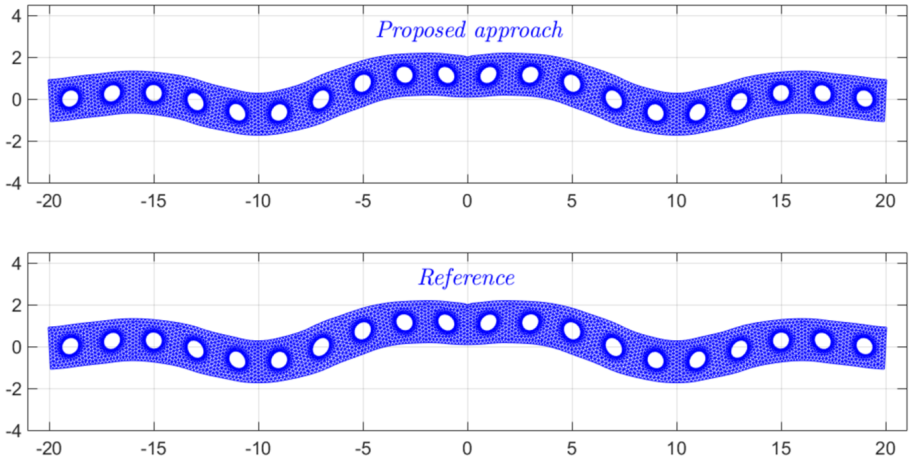

Figure 12: Periodic structure (square substructures with holes) subject to a Ricker wavelet pulse: deformed shape at $t = 0.01$ s.

right boundaries. Each substructure therefore includes a soft layer surrounding a stiff core, and in this sense, it is likely to behave in a more complicated way than previously.

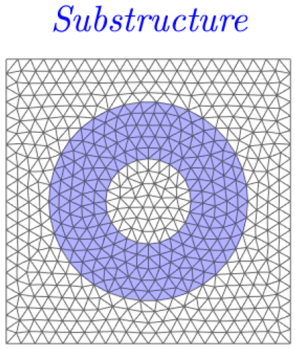

Figure 13: FE mesh of a substructure with a circular rubber layer (in blue).

Again, the time response of an infinite periodic structure consisting of an infinite number of substructures lying on periodic elastic supports (stiffness $K_s = 10^5$ N/m) is analyzed, in a quite analogous way than previously (see Fig. 8). Here, the structure is subject to a vertical point force $F_0(t)$ ($x = 0$, top node) which represents a Ricker wavelet force pulse whose expression is similar to Eq. (52). Concerning the proposed approach, a periodic structure involving $N = 20$ substructures and absorbing BCs is considered (as before, see Fig. 8). In this case, the rational approximations of the impedance matrices $\mathbf{Z}_L$ and $\mathbf{Z}_R$ (Eq. (11)) are expressed by means of $P = 19$ poles/residues. Also, for comparison purposes, an equivalent FE model with 200 substructures is considered.

The time response of the structure (time range of $[0\,,\,0.1]$ s) issued from the proposed approach is displayed in Fig. 14 along with the FE solution. In this case again, the proposed approach succeeds in predicting the dynamic behavior of the periodic structure over the whole time period. Fig. 14 shows the time variation of the transverse displacement at $x = 20$ m (right boundary, top node). The curve exhibits a main oscillation (say, between 0.02 s and 0.03 s) followed by several other oscillations of lower magnitudes which reflect the internal dynamic behavior of the substructures (motion of the cores embedded in the rubber layers). A closer look reveals that the deformed shape of the periodic structure, obtained via the proposed approach (e.g., at $t = 0.01$ s) also perfectly matches the reference solution, as shown in Fig. 15 where, for a better focus, only the deformations of the 10 central

substructures are shown. Especially, the "core motion" phenomenon inside the substructures is well highlighted. In this case, the relative error made for computing the displacement vector of the periodic structure with the proposed approach (Eq. (51)) is $\texttt{err} = 0.83\%$.

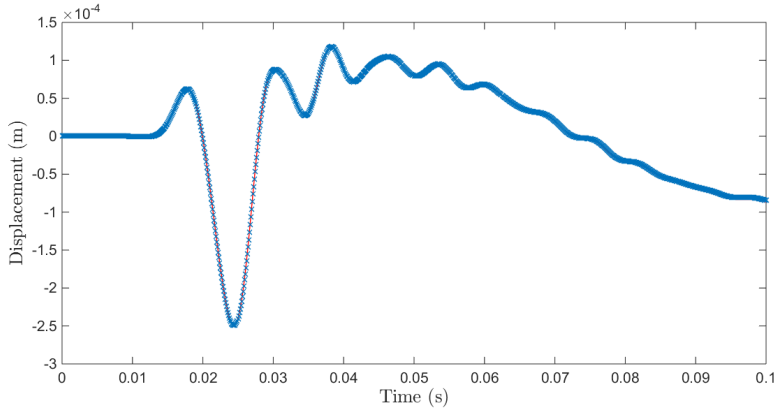

Figure 14: Periodic structure (square substructures with circular rubber layers) subject to a Ricker wavelet pulse: time response at $x = L/2$ (top node, vertical displacement). (blue crosses) Proposed approach; (red line) reference FE method.

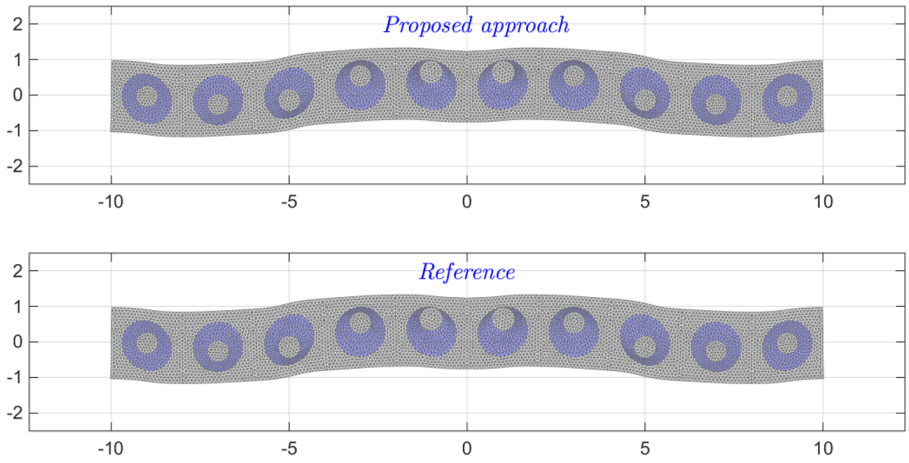

Figure 15: Periodic structure (square substructures with circular rubber layers) subject to a Ricker wavelet pulse: deformed shape at $t = 0.01$ s.

5. Conclusion

A FE procedure has been proposed to model infinite periodic structures subject to localized time-dependent excitations. This involves considering a structure with a finite number of substructures encompassing the excitations, and absorbing BCs to model semi-infinite structures outside the excitation region. The WFE method has been used to express the absorbing BCs by means of impedance matrices, in the frequency domain. Those impedance matrices have been rewritten in terms of polynomials of the frequency $\texttt{i}\omega$ up to order 2 which can be simply converted to the time domain. The procedure works by decomposing the impedance matrices in terms of rational functions, and by adding vectors of supplementary variables. As a result, a periodic structure can be modeled using a classical second-order time differential equation which can be integrated with the Newmark algorithm. Numerical experiments have been proposed which have clearly demonstrated the accuracy of the approach.

Several test cases have been considered which concern an infinite Euler-Bernoulli beam on an elastic foundation subject to a point harmonic force, and two periodic structures with 2D substructures subject to different kinds of point forces (harmonic force and Ricker wavelet). Follow-on works could include the analysis of infinite periodic structures with localized nonlinear effects, e.g., subject to fast loadings of high magnitudes (shocks, blast).

References

[1] R. Nelson, S. Dong, R. Kalra, Vibrations and waves in laminated orthotropic circular cylinders, Journal of Sound and Vibration 18 (3) (1971) 429–444.

[2] B. Aalami, Waves in Prismatic Guides of Arbitrary Cross Section, Journal of Applied Mechanics 40 (4) (1973) 1067–1072.

[3] L. Gavric, Computation of propagative waves in free rail using a finite element technique, Journal of Sound and Vibration 185 (3) (1995) 531–543.

[4] P. J. Shorter, Wave propagation and damping in linear viscoelastic laminates, The Journal of the Acoustical Society of America 115 (5) (2004) 1917–1925.

[5] I. Bartoli, A. Marzani, F. Lanza di Scalea, E. Viola, Modeling wave propagation in damped waveguides of arbitrary cross-section, Journal of Sound and Vibration 295 (3) (2006) 685–707.

[6] F. Treyssède, L. Laguerre, Investigation of elastic modes propagating in multi-wire helical waveguides, Journal of Sound and Vibration 329 (10) (2010) 1702–1716.

[7] W. Li, R. A. Dwight, T. Zhang, On the study of vibration of a supported railway rail using the semi-analytical finite element method, Journal of Sound and Vibration 345 (2015) 121–145.

[8] B. Mace, D. Duhamel, M. Brennan, L. Hinke, Finite element prediction of wave motion in structural waveguides, Journal of the Acoustical Society of America 117 (2005) 2835–2843.

[9] D. Duhamel, B. R. Mace, M. J. Brennan, Finite element analysis of the vibrations of waveguides and periodic structures, Journal of Sound and Vibration 294 (1-2) (2006) 205–220.

[10] J.-M. Mencik, D. Duhamel, A wave-based model reduction technique for the description of the dynamic behavior of periodic structures involving arbitrary-shaped substructures and large-sized finite element models, Finite Elements in Analysis and Design 101 (2015) 1–14.

[11] J.-M. Mencik, M. N. Ichchou, Multi-mode propagation and diffusion in structures through finite elements, European Journal of Mechanics - A/Solids 24 (5) (2005) 877–898.

[12] J.-M. Mencik, D. Duhamel, A wave finite element-based approach for the modeling of periodic structures with local perturbations, Finite Elements in Analysis and Design 121 (2016) 40 – 51.

[13] J.-M. Mencik, New advances in the forced response computation of periodic structures using the wave finite element (WFE) method, Computational Mechanics 54 (3) (2014) 789–801.

[14] J.-M. Mencik, A model reduction strategy for computing the forced response of elastic waveguides using the wave finite element method, Computer Methods in Applied Mechanics and Engineering 229-232 (2012) 68–86.

[15] J.-M. Mencik, A wave finite element approach for the analysis of periodic structures with cyclic symmetry in dynamic substructuring, Journal of Sound and Vibration 431 (2018) 441–457.

[16] M. N. Ichchou, J.-M. Mencik, W. J. Zhou, Wave finite elements for low and mid-frequency description of coupled structures with damage, Computer Methods in Applied Mechanics and Engineering 198 (15-16) (2009) 1311–1326.

[17] T. Hoang, D. Duhamel, G. Foret, Wave finite element method for waveguides and periodic structures subjected to arbitrary loads, Finite Elements in Analysis and Design 179 (2020) 103437.

[18] J. M. Renno, B. R. Mace, On the forced response of waveguides using the wave and finite element method, Journal of Sound and Vibration 329 (26) (2010) 5474 – 5488.

[19] Y. Waki, B. Mace, M. Brennan, Free and forced vibrations of a tyre using a wave/finite element approach, Journal of Sound and Vibration 323 (3) (2009) 737 – 756.

[20] R. Singh, C. Droz, M. Ichchou, F. Franco, O. Bareille, S. De Rosa, Stochastic wave finite element quadratic formulation for periodic media: 1D and 2D, Mechanical Systems and Signal Processing 136 (2020) 106431.

[21] Y. Fan, C. Zhou, J. Laine, M. Ichchou, L. Li, Model reduction schemes for the wave and finite element method using the free modes of a unit cell, Computers & Structures 197 (2018) 42 – 57.

[22] B. Engquist, A. Majda, Absorbing boundary conditions for numerical simulation of waves, Proceedings of the National Academy of Sciences 74 (5) (1977) 1765–1766.

[23] B. Engquist, A. Majda, Absorbing boundary conditions for numerical simulation of waves, Mathematics of Computation 31 (139) (1977) 629–651.

[24] R. Clayton, B. Engquist, Absorbing boundary conditions for acoustic and elastic wave equations, Bulletin of the Seismological Society of America 67 (6) (1977) 1529–1540.

[25] A. C. Reynolds, Boundary conditions for the numerical solution of wave propagation problems, Geophysics 43 (6) (1978) 1099–1110.

[26] A. Bayliss, E. Turkel, Radiation boundary conditions for wave-like equations, Communications on Pure and Applied Mathematics 33 (6) (1980) 707–725.

[27] R. Higdon, Absorbing boundary conditions for difference approximations to the multidimensional wave equation, Mathematics of Computation 47 (176) (1986) 437–459.

[28] R. Higdon, Numerical absorbing boundary conditions for the wave equation, Mathematics of Computation 49 (179) (1987) 65–90.

[29] F. Collino, High-order absorbing boundary conditions for wave propagation models. straight line boundary and corner cases, in: Proc. 2nd Int. Conf. on Mathematical & Numerical Aspects of Wave Propagation, R. Kleinmanet al.SIAM, Delaware, USA, 1993, pp. 161–171.

[30] T. Hagstrom, S. Hariharan, A formulation of asymptotic and exact boundary conditions using local operators, Applied Numerical Mathematics 27 (4) (1998) 403 – 416.

[31] J. Lee, J. Tassoulas, Absorbing boundary condition for scalar-wave propagation problems in infinite media based on a root-finding algorithm, Computer Methods in Applied Mechanics and Engineering 330 (2018) 207–219.

[32] J. Berenger, A perfectly matched layer for the absorption of electromagnetic waves, Journal of computational physics 114 (2) (1994) 185–200.

[33] J. Berenger, Three-dimensional perfectly matched layer for the absorption of electromagnetic waves, Journal of computational physics 127 (2) (1996) 363–379.

[34] F. Collino, P. Monk, Optimizing the perfectly matched layer, Computer methods in applied mechanics and engineering 164 (1) (1998) 157–171.

[35] S. Asvadurov, V. Druskin, M. Guddati, L. Knizhnerman, On optimal finite-difference approximation of PML, SIAM Journal on Numerical Analysis 41 (1) (2003) 287–305.

[36] F. Baida, A. Belkhir, Finite Difference Time Domain Method For Grating Structures, in: E. Popov (Ed.), Gratings: Theory and Numeric Applications, AMU (PUP), 2012, pp. 9.1–9.36.

[37] J. Li, Y. Huang, Time-Domain Finite Element Methods for Maxwell's Equations in Metamaterials, Springer Publishing Company, 2013.

[38] A. Deinega, I. Valuev, Long-time behavior of PML absorbing boundaries for layered periodic structures, Computer Physics Communications 182 (1) (2011) 149–151.

[39] G. Zheng, A. Kishk, A. Glisson, A. Yakovlev, Implementation of Mur's absorbing boundaries with periodic structures to speed up the design process using finite-difference time-domain method, Progress In Electromagnetics Research 58 (2006) 101–114.

[40] Y. Gao, P. Li, Analysis of time-domain scattering by periodic structures, Journal of Differential Equations 261 (9) (2016) 5094–5118.

[41] G. Marrocco, F. Capolino, Transient radiation by periodic structures: Accuracy of the (time domain-floquet wave)-fdtd algorithm, IEEE Antennas and Propagation Society, AP-S International Symposium (Digest) 3 (2002) 643–646.

[42] K. Sirenko, Y. Sirenko, H. Bagci, Exact absorbing boundary conditions for periodic three-dimensional structures: Derivation and implementation in discontinuous Galerkin time-domain method, IEEE Journal on Multiscale and Multiphysics Computational Techniques 3 (2018) 108–120.

[43] P. Ruge, C. Birk, A comparison of infinite Timoshenko and Euler-Bernoulli beam models on Winkler foundation in the frequency- and time-domain, Journal of Sound and Vibration 304 (3) (2007) 932 – 947.

[44] M. Zhao, L. Wu, X. Du, Z. Zhong, C. Xu, L. Li, Stable high-order absorbing boundary condition based on new continued fraction for scalar wave propagation in unbounded multilayer media, Computer Methods in Applied Mechanics and Engineering 334 (2018) 111 – 137.

[45] B. Weber, Rational transmitting boundaries for time-domain analysis of dam-reservoir interaction, Ph.D. thesis, ETH Zurich (1994).

[46] J. Yang, D. J. Thompson, A non-reflecting boundary for use in a finite element beam model of a railway track, Journal of Sound and Vibration 337 (2015) 199–217.

[47] W. X. Zhong, F. W. Williams, On the direct solution of wave propagation for repetitive structures, Journal of Sound and Vibration 181 (3) (1995) 485–501.

[48] K. Willcox, J. Peraire, Balanced model reduction via the proper orthogonal decomposition, AIAA Journal 40 (11) (2002) 2323–2330.

[49] S.-J. Moon, Rational function interpolation of electromagnetic transfer functions of high-speed interconnect systems from discrete time-domain and frequency-domain data, Ph.D. thesis, University of illinois (2009).

[50] R. Cottereau, D. Clouteau, C. Soize, Modèle dynamique équivalent de matrices d'impédance de fondation, in: 7-ème Colloque National de l'Association Française du Génie Parasismique, Chatenay Malabry, France, 2007, pp. 1–8.

[51] B. Gustavsen, Computer code for rational approximation of frequency dependent admittance matrices, IEEE Transactions on Power Delivery 17 (4) (2002) 1093–1098.

[52] V. Delavaud, A. Chaigne, F. Poisson, Rolling noise simulation: A new approach in time domain, in: T. Maeda, P.-E. Gautier, C. E. Hanson, B. Hemsworth, J. T. Nelson, B. Schulte-Werning, D. Thompson, P. de Vos (Eds.), Noise and Vibration Mitigation for Rail Transportation Systems, Springer Japan, Tokyo, 2012, pp. 61–69.

[53] L. Andersen, S.-R.-K. Nielsen, P.-H. Kirkegaard, Finite element modelling of infinite Euler beams on Kelvin foundations exposed to moving loads in convected co-ordinates, Journal of Sound and Vibration 241 (4) (2001) 587–604.

[54] Y. Feng, X. Wang, Matching boundary conditions for the Euler-Bernoulli beam, Shock and Vibration (2021) 6685852.

[55] G. Montseny, J. Audounet, D. Matignon, Fractional integro-differential boundary control of the Euler-Bernoulli beam, in: Proceedings of the 36th IEEE Conference on Decision and Control, Vol. 5, San Diego, US, 1997, pp. 4973–4978.

[56] S.-Q. Tang, E. Karpov, Artificial boundary conditions for Euler-Bernoulli beam equation, Acta Mechanica Sinica 30 (5) (2014) 687–692.

[57] F. Arbabi, M.-S. Farzanian, Propagation of waves in infinite beams: PML approach, in: 11th World Congress on Computational Mechanics (WCCM XI), Barcelona, Spain, 2014.

[58] P.-O. Persson, G. Strang, A Simple Mesh Generator in MATLAB, SIAM Rev. 46 (2) (2004) 329–345.